nature portfolio

Peer Review File

Heat-Driven Elastocaloric Cooling using Shape Memory Films

Corresponding Author: Professor Jingyuan Xu

Version 0:

Reviewer comments:

Reviewer #1

(Remarks to the Author)
The article describes an innovative concept for elastocaloric film-based cooling system driven by a heat source. Regarding the novelty of the concept, a similar one was proposed in reference 26, an elastocaloric cooling device with heat driven actuation, but in a regenerative configuration. Nonetheless, the proposed work here is very well described and the applicability of a heat driven actuation to a film-type elastocaloric cooler is of great interest. The experimental developments are particularly impressive, showing the careful design and dimensioning of the various sub-systems.
Please find below the main critical points to be addressed:
- In the introduction (line 58), reference 26 is cited to sustain the argument of a “large mass imbalance between drivetrains and refrigerants”, which is inadequate. Also, the force-displacement ratio should be defined. More generally speaking, the authors could have more deeply compared their results with the literature.
- The cooling power density is very large (5.49 W/g), but as the volume of SMA is very small, the net output cooling power remains very limited (2.83 mW). Commercial micro-coolers for thermal management of micro-electronic have a cooling power in the 1-100W range, mostly based on thermoelectric effect. The presented SMA heat driven cooler apparently intrinsically requires thin SMA layers (<1mm thickness). Hence, how far could we increase the quantity of SMA to increase the cooling power? What would be the impact on the device design and overall size?
- In COP determination, the step-by-step integration of the various sub-systems power consumption is a very good point of this work. However, the system also requires additional electromechanical actuators for moving cyclically the SMA films in contact to the heat sinks/source. Their power consumption should be considered too.
- SMA are known to exhibit a limited fatigue life in tensile stress actuation. A mention to literature data (if any) would be appreciated to give an idea of the fatigue life of both actuation SMA and cooling SMA.
- An adiabatic temperature change of 12.9 K for the SMA (when loaded by the heat driven actuator) is given in the abstract and in Suppl. Fig. 4. This value is misleading, as in Suppl. Fig. 4 the SMA film is not in adiabatic condition. A quasi-adiabatic condition may be considered only right after the temperature peaks. For the first peak, the amplitude is about ~8 K. When cooling the SMA actuator, a negative temperature peak is observed, but with a very different waveform, likely to be due to the thermal time constants that differ for heating and cooling the SMA actuator. This point could be discussed.
- Fig. 3, the authors calculated the temperature difference between heat sink and heat source, the first one being insulated and not thermally controlled. In the case of practical cooling the heat sink should be maintained near room temperature, so that the temperature span will probably decrease because of the increase of the thermal loss at the heat source level.

Reviewer #2

(Remarks to the Author)
This manuscript presents the first thin-film-based heat-driven elastocaloric cooling system, wherein thermal energy actuates a shape memory alloy (SMA) to induce elastocaloric cooling. The authors report a temperature span of 12.9 K at the refrigerant film level and 4.0 K at the device level under an 86 °C heat input, alongside a specific cooling power of 5.49 W g^{-1} and a coefficient of performance (COP) of 4.02. While the overarching concept of heat-driven elastocaloric cooling is both important and promising, the claimed novelties are undermined by three critical issues that limit the manuscript's significance.

The concept is not new. The authors repeatedly describe their actuation method as novel. However, the use of SMA as a thermal actuator for elastocaloric cooling has been previously introduced, e.g., ref. [26]. The thin-film geometry is indeed a new implementation, but its selection appears suboptimal. The slow thermal response of the heat actuator (<1 Hz, Fig. 4b) is incompatible with the high-frequency potential of microfilm-based cooling. For instance, TiNiFe films have demonstrated ~19 W g^{-1} specific cooling power at 4 Hz when driven by an electric motor as authors showed in ref. [16]. Without leveraging the frequency advantage, the thin-film configuration suffers from increased heat leakage, which diminishes its practical utility.

Exaggerated performance metrics. Key performance indicators, including cooling power, COP, and exergy efficiency, are incorrectly measured or calculated. The calculated cooling power only showed the microfilm TiNiFe provided ~3 mW cooling to the heat source, which balanced its own internal energy change during the initial cooling stage and heat leak to the ambient during the equilibrium state, yielding no net cooling from the heat source. From a system-level perspective, the effective cooling power should be considered zero, consistent with standard practice in the field. Furthermore, the COP is overstated, as it excludes the electrical input required to drive the heat source/sink. These omissions significantly weaken the claimed performance and novelty.

Inappropriate heat source representation The authors justify their concept by referencing low-grade heat sources such as waste heat and solar thermal energy. However, the experimental setup relies on Joule heating within the actuator, which differs fundamentally in heat transfer behavior. Joule heating produces a parabolic temperature profile due to a uniform internal generation, whereas external heat sources yield linear profiles from boundary heating. This discrepancy becomes increasingly relevant when scaling the system, casting doubt on the validity of the actuator's performance and the broader applicability of the proposed concept.

Minor Comments

The statement "Loading times are limited to ~500 ms and showed little improvement with higher currents or longer pulses" is insufficiently supported. Only data for 0.9 A and 1 A are shown in Supplementary Fig. 3a. A comprehensive dataset is needed to substantiate this claim.

The manuscript lacks an uncertainty analysis. Quantitative uncertainties for temperature, cooling power, and COP should be provided.

The use of a one-way SMA actuator prevents recovery of unloading work from the superelastic film. The authors should either revise the COP calculation to exclude work recovery or demonstrate a two-way SMA configuration.

The scalability of the proposed system remains unclear. Applications shown in Supplementary Fig. 6 require cooling powers ranging from several watts to hundreds of watts, which are not addressed in the current design.

Reviewer #3

(Remarks to the Author)
This submission describes an interesting and elegant strategy to achieve cooling without minimal use of electricity. The authors used a thermally powered TiNi thin strip to induce the elastocaloric effect in a TiNiFe thin strip, coupled with controlled movement of a heat sink for the actuating strip and a pair of heat sink and source for the elastocaloric TiNiFe thin strip. Although the device presented does not appear to be a complete cooler system, the concept points to a new approach to harvesting waste or environmental heat for thermal management. The paper could be suitable for publication after the comments are addressed:

1. The actuator and refrigerant films form a push-pull couple. As the stroke of 300 um is much greater than the film thickness, buckling could occur when a film is pushed. Was buckling observed, and how was it overcome?

2. In the cooling device, the actuator is activated via Joule heating. It is recommended to use a direct heat source to activate the actuator? It is understandably that the heating using external heat would be slow, but it is important to demonstrate such truly thermally driven cooling. How about using hot and cold water to drive the actuator?

3. It is unclear how rapid heat transfer between the SMA films and the heat sinks and source was obtained. Provide relevant experimental details with illustration or images to facilitate the description.

4. Provide information of the operating stability of the device? How many cycles can this device run without an obvious deterioration in its cooling performance?

5. What is the total length and width of the TiNiFe film in the cooling unit?

6. What is the speed of the stretching that the actuator film can generate when it is coupled to the refrigerant film? Can faster stretching speed of the actuator film result in a larger adiabatic temperature change in the refrigerant film and thus better performance at the device level?

7. Questions about the temperature span/cooling power measurement:
a. A miniaturized thermocouple is attached to the backside of the Cu heat sink to measure the temperature. What is the size of this thermocouple and how do you ensure that the temperature profile along the Cu heat sink is uniform and the reading of thermocouple can reflect the actual temperature of the Cu strip?
b. Can you show the detailed calculation of the cooling power (the specific numbers you plugged in Q = msourcecp, sourceTsource)?
c. Is it possible for you to use a heat flux sensor to measure the cooling power? This measurement would be more direct.
d. What causes the large discrepancy between the material temperature span and the device temperature span?
e. If you use a Cu heat sink with a larger heat mass (for example, a thicker Cu strip) but the heat source stays unchanged,

could a larger temperature span or more cooling be obtained in the heat source?

Reviewer #4

(Remarks to the Author)
This submission describes an interesting and elegant strategy to achieve cooling without minimal use of electricity. The authors used a thermally powered TiNi thin strip to induce the elastocaloric effect in a TiNiFe thin strip, coupled with controlled movement of a heat sink for the actuating strip and a pair of heat sink and source for the elastocaloric TiNiFe thin strip. Although the device presented does not appear to be a complete cooler system, the concept points to a new approach to harvesting waste or environmental heat for thermal management. The paper could be suitable for publication after the comments are addressed:

1. The actuator and refrigerant films form a push-pull couple. As the stroke of 300 um is much greater than the film thickness, buckling could occur when a film is pushed. Was buckling observed, and how was it overcome?

2. In the cooling device, the actuator is activated via Joule heating. It is recommended to use a direct heat source to activate the actuator? It is understandably that the heating using external heat would be slow, but it is important to demonstrate such truly thermally driven cooling. How about using hot and cold water to drive the actuator?

3. It is unclear how rapid heat transfer between the SMA films and the heat sinks and source was obtained. Provide relevant experimental details with illustration or images to facilitate the description.

4. Provide information of the operating stability of the device? How many cycles can this device run without an obvious deterioration in its cooling performance?

5. What is the total length and width of the TiNiFe film in the cooling unit?

6. What is the speed of the stretching that the actuator film can generate when it is coupled to the refrigerant film? Can faster stretching speed of the actuator film result in a larger adiabatic temperature change in the refrigerant film and thus better performance at the device level?

7. Questions about the temperature span/cooling power measurement:
a. A miniaturized thermocouple is attached to the backside of the Cu heat sink to measure the temperature. What is the size of this thermocouple and how do you ensure that the temperature profile along the Cu heat sink is uniform and the reading of thermocouple can reflect the actual temperature of the Cu strip?
b. Can you show the detailed calculation of the cooling power (the specific numbers you plugged in Q = msourcecp, sourceTsource)?
c. Is it possible for you to use a heat flux sensor to measure the cooling power? This measurement would be more direct.
d. What causes the large discrepancy between the material temperature span and the device temperature span?
e. If you use a Cu heat sink with a larger heat mass (for example, a thicker Cu strip) but the heat source stays unchanged, could a larger temperature span or more cooling be obtained in the heat source?

Version 1:

Reviewer comments:

Reviewer #1

(Remarks to the Author)
The authors significantly improved their manuscript with a clear point-to-point reply to the reviewer's comment. Therefore, it can be recommended for publication.

Reviewer #2

(Remarks to the Author)
The authors have substantially expanded the manuscript by adding new experimental data, supplementary materials, and demonstrations of heat-driven cooling using an external heat source. They have also provided detailed responses to the concerns raised by all three referees. These additions improve the clarity and completeness of the work, and the revised version reads significantly better than the original submission.
However, several of the newly added materials still contain technical inconsistencies or incomplete explanations. The authors must address the following issues before the manuscript can meet the publication standards of Nature Energy.
1. The authors should include video documentation of the prototype operating with the external heat source to maintain consistency with the Joule-heated demonstration.
2. The expanded discussion of COP and exergetic efficiency is valuable, but key information is still missing. Specifically, the transient development of the temperature span under different external loads shown in Supplementary Fig. 7 should be

added, and the temperatures used to calculate exergetic efficiency should be included in Supplementary Table 4.
3. In Supplementary Fig. 7, the noticeable discrepancy between the green dot and the blue diamond at 0 K requires further clarification to ensure the accuracy of the presented trends.
4. The caption of Supplementary Fig. 9 refers to operation "without active heat-sink implementation" and to "significant variability due to uncontrolled convective cooling," but it is unclear whether this means the SMA dissipates heat directly to ambient air without contacting a heat sink, and this ambiguity should be resolved. Moreover, the claim that the results "highlight the potential of low-grade thermal energy" is not supported given that the revised experiments require a substantially higher driving temperature of 130 °C compared to 86 °C in the Joule-heated case.
5. The response regarding scalability remains insufficient, as citing two approaches from prior work does not address the core issue that distributing external heat uniformly across multiple SMA elements in a parallel configuration introduces additional thermal resistance that is not accounted for in the current proof-of-concept system.
6. The trends in Supplementary Fig. 4 and Fig. 6 are inconsistent, since Tc is always lower when the heat sink is at Tamb in Fig. 4, whereas the opposite trend appears in Fig. 6, and this contradiction must be resolved.
7. Supplementary Note 1 introduces the force-displacement ratio, but the manuscript does not specify the ideal target value or how closely the demonstrated system approaches it, and this metric requires clearer explanation.
8. Supplementary Note 3 conflates efficiency and COP, even though efficiency cannot exceed 100% while COP can, and the authors should revise this section to avoid conceptual confusion.
9. The notation for temperature differences should be used consistently throughout the manuscript - either T0 - Tc or Tc - T0.
10. The COPs and exergetic efficiencies in Supplementary Table 4 should be reported with consistent significant digits.

Reviewer #3

(Remarks to the Author)
The authors have adequately addressed the concerns raised during the previous review process. They have incorporated a direct heat source to activate the actuator, clarified the significant discrepancy between device-level and material-level temperature variations, analyzed the heat transfer rates among different components, and demonstrated the mechanical operation and stability of the device. Additionally, they have supplied supplementary details regarding precise device dimensions, comprehensive calculations of cooling power, measurements of cooling temperature on the cold side, and temperature lift assessments. Accordingly, this paper is now suitable for publication in Nature Energy.

Reviewer #4

(Remarks to the Author)
The authors have adequately addressed the concerns raised during the previous review process. They have incorporated a direct heat source to activate the actuator, clarified the significant discrepancy between device-level and material-level temperature variations, analyzed the heat transfer rates among different components, and demonstrated the mechanical operation and stability of the device. Additionally, they have supplied supplementary details regarding precise device dimensions, comprehensive calculations of cooling power, measurements of cooling temperature on the cold side, and temperature lift assessments. Accordingly, this paper is suitable for publication in Nature Energy.

Version 2:

Reviewer comments:

Reviewer #2

(Remarks to the Author)
The reviewers have addressed my comments but two revisions are not satisfactory.

First, the new video 4 is helpful, but for consistency, please also add the video of the refrigerant film in the case of external heat source.

Second, the added transient data in supplementary fig. 7b is useful. Based on those trend, the temperature span is still developing and full cyclic equilibrium is not reached yet. Why would the authors stop testing prematurely? Please provide relavant information and it will be beneficial to the field.

Response Letter

Reviewer 1's comments

<u>Comment 1</u>: *The article describes an innovative concept for elastocaloric film-based cooling system driven by a heat source. Regarding the novelty of the concept, a similar one was proposed in reference 26, an elastocaloric cooling device with heat driven actuation, but in a regenerative configuration. Nonetheless, the proposed work here is very well described and the applicability of a heat driven actuation to a film-type elastocaloric cooler is of great interest. The experimental developments are particularly impressive, showing the careful design and dimensioning of the various sub-systems.*

Response: We sincerely thank the Reviewer for the positive evaluation of our work and for recognizing the relevance of heat-driven actuation for film-based elastocaloric cooling. We also appreciate the opportunity to further clarify the relationship to Ref. [26].

As noted by the Reviewer, Ref. [26] proposed a regenerative heat-driven elastocaloric architecture based on thermodynamic modeling and numerical simulation at macroscopic scale. In the revised manuscript, we have explicitly clarified this distinction. Specifically, while Ref. [26] provides important theoretical insights into thermally driven elastocaloric cycles, the present study focuses on the experimental realization of thermally powered shape-memory actuation directly coupled to a thin-film elastocaloric refrigerant within a miniaturized prototype. The key advances of this work lie in: (i) implementation using micrometer-thick SMA films, (ii) force–displacement matching between actuator and refrigerant at miniature scale, and (iii) integrated device-level validation of heat-driven cooling performance. These distinctions are now clearly articulated in the Introduction to avoid any implication of conceptual exclusivity and to appropriately position our contribution as an experimental realization and miniaturized implementation.

Following the Editor's guidance, we have also removed priority-based wording (e.g., "new", "novel", "first") throughout the manuscript and refined the language to emphasize demonstrated technological advances rather than claims of conceptual precedence.

Changes made:

- Added a paragraph in the *Introduction* (Page 2, Line 77–84) explicitly clarifying the distinction from Ref. [26]:

"A regenerative heat-driven elastocaloric concept has previously been proposed through thermodynamic modeling and numerical simulations at macroscopic scale[26], providing important theoretical insights into cycle design and energy flow. In contrast, the present work experimentally realizes thermally powered shape-memory actuation directly coupled to a thin-film elastocaloric refrigerant architecture at miniature scale. The integrated prototype achieves a 12.9 K temperature span at the material level and a 4.0 K temperature span at the device level under Joule-heated thermal actuation at 86 °C, providing an experimental demonstration of film-based heat-driven elastocaloric cooling.".

- Removed priority-based wording (e.g., "new", "novel", "first") throughout the *Abstract*, *Introduction*, *Results*, and *Conclusion*.

Comment 2: *In the introduction (line 58), reference 26 is cited to sustain the argument of a "large mass imbalance between drivetrains and refrigerants", which is inadequate. Also, the force-displacement ratio should be defined. More generally speaking, the authors could have more deeply compared their results with the literature.*

Response: We thank the Reviewer for this careful and constructive comment.

First, we agree that the previous citation of Ref. [26] to support the statement regarding "large mass imbalance" was not sufficiently precise. In the revised manuscript, this discussion has been clarified and reformulated. The statement is now presented as a general mechanical design consideration arising from the use of conventional electromechanical drivetrains relative to thin-film refrigerants, rather than being specifically attributed to Ref. [26].

Second, we have now explicitly defined the force–displacement ratio at its first occurrence in the Introduction. It is defined as the ratio between the maximum output force and the corresponding stroke length of an actuator. This definition clarifies its relevance for superelastic SMA refrigerants, which require high force over limited displacement due to their high transformation stress and small strain window.

Third, quantitative comparisons of force–displacement ratios (14.5 for the developed SMA-based thermal actuator in this work versus 1.1 of the representative commercial actuator used in this study) and device-level temperature spans are now more explicitly discussed to better position our results within the broader elastocaloric research landscape. Detail explanation and calculation method of the force–displacement ratio is discussed in Supplementary Note 1.

Changes made:

- Revised the discussion of actuator–refrigerant mass imbalance and added explicit definition of force–displacement ratio at its first occurrence in the *Introduction* (Page 2, Line 55–63):

"However, high-force actuators are commonly designed for long stroke operation, resulting in relatively low force–displacement ratios (defined here as the ratio between maximum output force and stroke length). In contrast, superelastic SMA refrigerants require stresses on the order of several hundred MPa while undergoing only a few percent strain, thereby demanding high force over limited displacement and corresponding to a high force–displacement ratio. This mismatch in actuator–refrigerant mechanical characteristics, together with the substantial mass of conventional drivetrains relative to thin-film refrigerants, leads to inefficient drivetrain utilization and oversized actuation systems."

- Expanded quantitative comparison of actuator mechanical characteristics in the *Introduction* (Page 2, Line 71–76):

"The SMA-based thermal actuator provides improved force–displacement matching to the refrigerant, achieving a force–displacement ratio of 14.5, compared with 1.1 for the commercial electromechanical actuator used in this study (Supplementary Note 1). This improved matching arises from the intrinsic shape recovery behavior of high-temperature SMAs, which enables high force generation over limited stroke without the need for bulky gearboxes or mechanical transmission systems[26,28–34]."

Comment 3: *The cooling power density is very large (5.49 W/g), but as the volume of SMA is very small, the net output cooling power remains very limited (2.83 mW). Commercial micro-coolers for thermal management of micro-electronic have a cooling power in the 1-100W range, mostly based on thermoelectric effect. The presented SMA heat driven cooler apparently intrinsically requires thin SMA layers (<1mm thickness). Hence, how far could we increase the quantity of SMA to increase the cooling power? What would be the impact on the device design and overall size?*

Response: We thank the Reviewer for this important comment regarding cooling power magnitude and scalability toward practical thermal management applications.

We agree that although the specific cooling power is high, the absolute cooling power (2.79 mW) is limited by the small active mass of the present thin-film prototype. The current device was intentionally designed as a miniature proof-of-concept to validate thermally driven actuation and film-level integration, rather than to maximize absolute cooling capacity.

To address scalability, we have expanded the Discussion to clarify feasible upscaling strategies based on established film-based elastocaloric architectures. In particular:

- Parallelization of multiple films: As demonstrated by Ulpiani *et al.* (Ref. [19]), increasing the number of SMA films in parallel can proportionally increase cooling capacity. Their proof-of-concept parallel demonstrator increased cooling power by a factor of 4.5 when scaling from one to five films, reaching 0.9 W.
- Increasing lateral film dimensions: Because the elastocaloric effect scales with active material volume while maintaining similar strain amplitude and stress levels, enlarging film width and active length increases total cooling power approximately proportionally, provided heat transfer rates remain sufficient.
- Modular integration: For thin-film architectures, multiple film stacks can share common heat sinks and heat sources, which mitigates footprint growth compared to duplicating full device assemblies.

We have also clarified that increasing film number and lateral size introduces additional design challenges, including synchronization of heat exchanger motion, uniform stress distribution across multiple films, and maintaining effective heat transfer rates at higher total cooling power. These engineering considerations are now explicitly discussed to provide a balanced perspective on scalability. Importantly, we position the present work as establishing the feasibility of thermally driven thin-film elastocaloric cooling, with a scaling pathway analogous to previously demonstrated parallel film-based systems, rather than as a direct competitor to watt-level commercial thermoelectric modules.

Reference:

[19] Ulpiani, G. *et al.* Upscaling of SMA film-based elastocaloric cooling. *Applied Thermal Engineering* **180**, 115867 (2020).

Changes made:

- Expanded the *Discussion* to clarify scalability pathways as well as engineering constraints associated with scaling (Page 7, Line 276–287):

"The present prototype serves as a proof-of-concept platform for investigating scalability of film-based heat-driven elastocaloric cooling. Although the absolute cooling power is limited by the small active mass of the thin-film refrigerant, the total cooling capacity can be increased by (i) integrating multiple films in parallel and (ii) enlarging the lateral dimensions of each film, as demonstrated for film-based elastocaloric systems in Ref. 19. Because the cooling power scales approximately with the volume of actively cycled material under comparable stress and strain conditions, increasing the number or area of films can proportionally enhance total output. In the present architecture, modular integration with shared heat sinks and heat sources may mitigate footprint growth compared to duplicating complete device assemblies. However, scaling to higher cooling capacities will require careful control of actuator synchronization, uniform stress distribution across multiple films, and maintenance of efficient heat transfer at increased thermal loads.”.

Comment 4: *In COP determination, the step-by-step integration of the various sub-systems power consumption is a very good point of this work. However, the system also requires additional electromechanical actuators for moving cyclically the SMA films in contact to the heat sinks/source. Their power consumption should be considered too.*

Response: We thank the Reviewer for highlighting this important point. We agree that the electrical power consumption of the auxiliary electromechanical actuators used to cyclically move the heat exchangers should be considered for a complete system-level efficiency assessment. In the revised manuscript, we have therefore expanded the COP and exergetic efficiency analysis to include additional input-power definitions beyond the actuator thermal input basis. Specifically, we now account for:

- The electrical power consumption of the two auxiliary servo actuators responsible for heat-exchanger motion.
- The electrical power supplied for Joule heating of the actuator film,
- The power required to maintain the external heat-source temperature

When including these additional electrical inputs, the full-system COP decreases significantly compared to calculations based solely on actuator thermal input. For example, in the Joule-heated configuration, the full-system COP decreases from 0.09 (thermal input basis) to 0.02 when electrical Joule heating power is used as input, and further to $\sim 7\times10^{-4}$ when auxiliary actuator power is included. Similar trends are observed for the externally heat-driven configuration.

We note that the present prototype employs high-precision laboratory servo actuators to enable flexible experimental control and operating range. These components consume substantially more power than would be required in a purpose-designed compact system. Therefore, while the expanded analysis provides a transparent and comprehensive accounting of total electrical input, it represents a prototyping scenario rather than an optimized device architecture.

All expanded calculations, definitions, and power-integration methods have been added to *Supplementary Note 3* and summarized in *Supplementary Table 4*.

Changes made:

- Expanded COP and exergetic efficiency analysis to include (i) power consumption of the auxiliary linear actuators used to move the heat exchangers, (ii) electrical power supplied for Joule heating, and (iii) input power required to maintain the external heat source.
- Added expanded system-level COP and exergetic efficiency results in *Supplementary Table 4*, summarizing all evaluation conditions, including cases where auxiliary actuator electrical consumption is incorporated.

- Added detailed formulations for COP and exergetic efficiency under different input-power bases in *Supplementary Note 3*, including explicit expressions for full-system evaluation with auxiliary actuator power consumption.

Supplementary Table 4. Coefficient of performance (COP) and exergetic efficiency of Joule-heated and externally heat-driven elastocaloric systems under different evaluation criteria. Definitions of COP and exergetic efficiency, including the corresponding input-power bases, are provided in Supplementary Note 3.

Evaluation conditions		COP	Exergetic efficiency
Joule heating actuation		evaluated at $T_c - T_0 = 0$ K	evaluated at $T_c - T_0 = -1$ K
Temperature-slope method	Cooler (with work recovery)	5.46	–
	Cooler (without work recovery)	2.88	–
	Thermal actuator efficiency (thermal input basis)	0.03	–
	Thermal actuator efficiency (electrical input basis)	0.01	–
	Full system (thermal input basis)	0.09	–
	Full system (electrical input basis)	0.02	–
	Full system (thermal input basis + auxiliary actuators)	0.0008	–
	Full system (electrical input basis + auxiliary actuators)	0.0007	–
Counter-heating method	Cooler (with work recovery)	4.94	4.21 %
	Cooler (without work recovery)	2.61	2.22 %
	Thermal actuator efficiency (thermal input basis)	0.03	3.27 %
	Thermal actuator efficiency (electrical input basis)	0.01	0.84 %
	Full system (thermal input basis)	0.09	0.07 %
	Full system (electrical input basis)	0.02	0.02 %
	Full system (thermal input basis + auxiliary actuators)	0.0007	0.001 %
	Full system (electrical input basis+ auxiliary actuators)	0.0007	0.001 %

External heat-source actuation		evaluated at $T_c - T_0 = 0$ K	evaluated at $T_c - T_0 = -0.5$ K
Temperature-slope method	Cooler (with work recovery)	2.31	–
	Cooler (without work recovery)	1.50	–
	Thermal actuator efficiency (electrical input basis)	0.0024	–
	Full system (electrical input basis)	0.0036	–
	Full system (electrical input basis+ auxiliary actuators)	0.0002	–
Counter-heating method	Cooler (with work recovery)	3.55	1.37 %
	Cooler without work recovery	2.31	0.89 %
	Thermal actuator efficiency (electrical input basis)	0.0024	0.24 %
	Full system (electrical input basis)	0.0056	0.002 %
	Full system (electrical input basis+ auxiliary actuators)	0.0003	< 0.001 %

Note:

- COP values reported for the full system correspond to the one-way shape memory actuator configuration without work recovery. Values labeled "with work recovery" represent a theoretical upper bound of the cooling unit and are provided for benchmarking future bidirectional actuator designs.
- For Joule-heated actuation, the full-system COP/exergetic efficiency on a thermal-input basis (including auxiliary actuators) and on an electrical-input basis (including auxiliary actuators) are identical (0.0007/0.001%). This equivalence arises from the dominant input power consumption of the auxiliary actuators combined with the relatively small cooling power measured via direct counter-heating.

Comment 5: *SMA are known to exhibit a limited fatigue life in tensile stress actuation. A mention to literature data (if any) would be appreciated to give an idea of the fatigue life of both actuation SMA and cooling SMA*

Response: We thank the Reviewer for raising this important point regarding fatigue life under tensile actuation, which is indeed critical for elastocaloric systems. In the revised manuscript, we have expanded the discussion of fatigue behavior for both the refrigerant and actuator films.

For the superelastic TiNiFe refrigerant film used in the present prototype, in-house fatigue testing was conducted under 5.2% tensile strain at a strain rate of 0.02 s^{-1}. The film sustained more than 2000 cycles without mechanical failure or observable functional degradation. While this initial demonstration was not designed as a long-term lifetime study, it confirms the mechanical robustness of the selected film under the operating strain range.

Importantly, extensive literature demonstrates that TiNi-based thin films can achieve ultra-low fatigue behavior under tensile loading. In particular, Ti-rich TiNiCu and TiNiCuCo thin films have been reported to withstand more than 10^7 cycles without functional degradation in elastocaloric operation (Refs. 42–44). These materials are directly compatible with thin-film architectures and provide a pathway toward substantially extended device lifetimes.

For the actuator film, similar TiNi-based thin films have been demonstrated to exhibit stable cyclic phase transformation under repeated thermal actuation in the same literature. Thus, both refrigerant and actuator elements can benefit from established ultra-low-fatigue alloy systems.

Reference:

[42] Chluba, C. *et al.* Ultralow-fatigue shape memory alloy films. *Science* **348**, 1004–1007 (2015).
[43] Chluba, C., Ossmer, H., Zamponi, C., Kohl, M. & Quandt, E. Ultra-Low Fatigue Quaternary TiNi-Based Films for Elastocaloric Cooling. *Shap. Mem. Superelasticity* **2**, 95–103 (2016).
[44] Ossmer, H., Chluba, C., Kauffmann-Weiss, S., Quandt, E. & Kohl, M. TiNi-based films for elastocaloric microcooling— Fatigue life and device performance. *APL Mater.* **4**, 064102 (2016).

Changes made:

- Added in-house fatigue test results for the TiNiFe refrigerant film as well as discussion of ultra-low-fatigue TiNi-based thin films in the *Methods* (Page 8, Line 351–363):

"The fatigue behavior of the superelastic TiNiFe refrigerant film was evaluated under tensile loading at 5.2% strain and a strain rate of 0.02 s^{-1}. The film sustained more than 2000 cycles without mechanical failure or observable functional degradation, confirming mechanical robustness within the operating strain range of the present prototype. However, the primary objective of this work was to establish a proof-of-concept demonstration of heat-driven elastocaloric cooling rather than to optimize long-term cyclic lifetime. Consequently, fatigue-optimized SMA compositions were not specifically implemented in the current device. Notably, ultra-low-fatigue TiNi-based thin films have been reported in the literature. Ti-rich TiNiCu and TiNiCuCo films have demonstrated stable cyclic performance exceeding 10^7 cycles under tensile actuation without functional degradation[42–44]. These alloy systems are fully compatible with thin-film elastocaloric architectures. Combined with improved mechanical design to minimize stress concentration and thermal accumulation, they provide a clear pathway toward substantially extending operational lifetime in future device generations.".

Comment 6: *An adiabatic temperature change of 12.9 K for the SMA (when loaded by the heat driven actuator) is given in the abstract and in Suppl. Fig. 4. This value is misleading, as in Suppl. Fig. 4 the SMA film is not in adiabatic condition. A quasi-adiabatic condition may be considered only right after the temperature peaks. For the first peak, the amplitude is about ~8 K. When cooling the SMA actuator, a negative temperature peak is observed, but with a very different waveform, likely to be due to the thermal time constants that differ for heating and cooling the SMA actuator. This point could be discussed.*

Response: We thank the Reviewer for this important and technically precise comment.

We agree that the previously stated 12.9 K value does not represent a fully adiabatic temperature change. In the revised manuscript, we have corrected the wording to clarify that the 12.9 K corresponds to a maximum material-level temperature change observed during loading, rather than a fully adiabatic temperature change. We now explicitly distinguish this transient response from the independently measured fully adiabatic temperature change of 19.4 K obtained under high strain-rate tensile testing (Supplementary Fig. 2), where heat exchange with the surroundings is minimized.

We have also expanded the discussion to address the asymmetry between heating and cooling peaks. The larger temperature rise during loading compared to the temperature drop during unloading arises from (i) the higher loading strain rate (0.09 s^{-1}) relative to the unloading strain rate (0.03 s^{-1}), and (ii) asymmetric thermal time constants governing heat exchange with the surroundings during heating and cooling. Under the present operating conditions, quasi-adiabatic behavior is approached only immediately after the temperature peak, before significant heat exchange occurs.

These clarifications have been incorporated into the revised *Supplementary Fig. 5* caption and the corresponding discussion in the manuscript.

Changes made:

- Corrected the wording in *Supplementary Fig. 5* to replace "adiabatic temperature change" with "maximum material-level temperature change under quasi-adiabatic conditions" and clarified the distinction between the quasi-adiabatic response (12.9 K) and the independently measured fully adiabatic temperature change of 19.4 K. The revised caption now states (Page 13):

"A maximum material-level ~~adiabatic~~ temperature change of 12.9 K is observed under quasi-adiabatic conditions. This value does not correspond to the fully adiabatic temperature change of 19.4 K measured independently under high strain-rate tensile testing (Supplementary Fig. 2). The temperature rise during loading exceeds the temperature drop during unloading due to the higher loading strain rate (0.09 s^{-1}) compared to the unloading strain rate (0.03 s^{-1}), as well as asymmetric thermal time constants governing heat exchange with the surroundings.".

- Added discussion of strain-rate asymmetry and thermal time-constant effects to explain the different heating and cooling waveforms in the *Methods* section (Page 10, Line 434–453):

"The material-level temperature change of 12.9 K for TiNiFe films under Joule-heated thermal actuation is lower than the fully adiabatic value of 19.4 K measured under high strain-rate tensile testing. This reduction arises from the limited strain rate during device operation. Likewise, the device-level temperature span of 4.0 K in the coupled heat-driven configuration remains below the maximum 8.2 K achieved in the cooling-only unit driven by an electromechanical actuator. In both cases, the limitation originates from thermally constrained actuation dynamics, which restrict both the strain rate and the achievable operating frequency. Fully adiabatic conditions typically require strain rates ≥ 0.1 s^{-1} (≈ 750 μm/s), whereas the present actuator provides 0.09 s^{-1} during loading (≈ 639 μm/s) and 0.07 s^{-1} during unloading (≈ 526 μm/s). These sub-adiabatic strain rates allow partial heat exchange during phase transformation. At the device level, the temperature span is further limited by finite heat-transfer rates between the refrigerant film and the heat sink/source, as well as the thermal mass of the heat exchangers during cyclic operation. In the absence of regenerative or cascaded architecture[15,45], the net temperature lift accumulated per cycle remains lower than the intrinsic material temperature change. Future improvements may focus on increasing strain rates through optimized actuator geometry, enhanced heat transfer, or alternative actuation strategies to more fully exploit the intrinsic cooling potential of the refrigerant film. Advanced actuation concepts, including bistable configurations, agonist–antagonist designs, or catch-and-release mechanisms[46,47], together with multistage cascading architectures on the cooling side[15,45], may further enhance the effective device-level temperature span.".

Comment 7: *Fig. 3, the authors calculated the temperature difference between heat sink and heat source, the first one being insulated and not thermally controlled. In the case of practical cooling the heat sink should be maintained near room temperature, so that the temperature span will probably decrease because of the increase of the thermal loss at the heat source level.*

Response: We thank the Reviewer for this important and application-oriented comment. We agree that, in practical cooling applications, the heat sink should be maintained close to ambient temperature rather than thermally insulated.

In the original configuration, the heat sink was insulated to assess the intrinsic maximum temperature span of the cooling unit under minimal boundary constraints. To address the Reviewer's concern, we performed additional experiments in which the heat sink was maintained within 1 K above ambient temperature using a higher thermal mass. Under this more application-relevant boundary condition, the overall temperature span (ΔT_{total}) decreases by approximately 2.0 K due to the reduced temperature rise on the hot side. However, the cold-side temperature drop ($T_c - T_0$) increases by an average of 0.8 K compared to the insulated condition. These additional results demonstrate that while the total temperature span is smaller under controlled boundary conditions, the effective cooling performance (cold-side temperature drop relative to ambient) improves, which is more relevant for practical applications.

Changes made:

- Added a discussion in the "*Elastocaloric cooling unit*" section (Page 5, Line 183−191) comparing insulated and ambient-controlled heat-sink boundary conditions:

"By maintaining the heat sink temperature within 1.0 K above ambient, representing a more application-relevant boundary condition, the cold-side temperature drop ($\Delta T_c = T_c - T_0$) increases by an average of 0.8 K compared to the insulated configuration (Supplementary Fig. 4). Although constraining the hot-side temperature rise reduces the overall temperature span ($\Delta T_{total} = T_h - T_c$), maintaining the heat sink near ambient prevents an upward shift of the system reference temperature and results in a larger measurable temperature drop relative to ambient conditions. Detailed temperature-span values under both insulated and ambient-controlled conditions are summarized in Supplementary Table 1."

- Added *Supplementary Fig. 4* showing temperature-drop comparison under insulated and ambient-controlled heat-sink conditions:

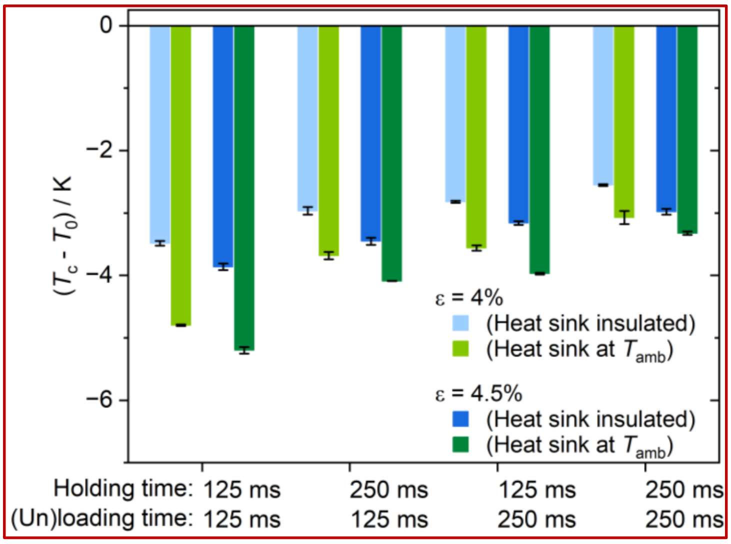

Supplementary Fig. 4. Comparison of temperature drop (T_c – T_0) under different heat-sink boundary conditions and strain ε. Temperature drops were measured using the stand-alone cooling unit driven by electromechanical actuators. Results are shown for ε = 4% and ε = 4.5% at different (un)loading and holding times (125 ms and 250 ms). Light blue and dark blue bars represent ε = 4% and ε = 4.5%, respectively, with the heat sink insulated. Light green and dark green bars represent ε = 4% and ε = 4.5%, respectively, with the heat sink maintained at ambient temperature (T_{amb}). Maintaining the heat sink near ambient temperature using a larger thermal mass (limiting the hot-side temperature rise to <1 K above ambient) increases the temperature drop by an average of 0.8 K compared to the insulated condition. Detailed numerical values are provided in Supplementary Table 1. Data are shown as mean ± standard deviation (n = 3 independent experiments).

- Added *Supplementary Table 1* summarizing ΔT_{total} and ($T_c - T_0$) for all tested strain and timing conditions:

Supplementary Table 1. Device-level total temperature span ($\Delta T_{total} = T_h - T_c$) and cold-side temperature drop ($\Delta T_c = T_c - T_0$) of the stand-alone elastocaloric cooling unit driven by electromechanical actuators under different boundary conditions, applied strain, and timing parameters. Holding/(un)loading time refers to the duration of thermal contact and mechanical loading/unloading, respectively.

Conditions					
Heat sink	Heat source	Strain ε	Holding/(Un)loading time (ms)	ΔT_{total} (K)	ΔT_c (K)
Insulated	Insulated	4.0 %	125 / 125	7.2	− 3.5
			250 / 125	6.0	− 3.0
			125 / 250	5.7	− 2.8
			250 / 250	5.1	− 2.6
		4.5 %	125 / 125	8.2	− 3.9
			250 / 125	7.2	− 3.5
			125 / 250	6.6	− 3.2
			250 / 250	6.1	− 3.0
Maintained at T_{amb}	Insulated	4.0 %	125 / 125	5.5	− 4.8
			250 / 125	4.2	− 3.7
			125 / 250	4.1	− 3.6
			250 / 250	3.5	− 3.1
		4.5 %	125 / 125	5.9	− 5.2
			250 / 125	4.7	− 4.1
			125 / 250	4.5	− 4.0
			250 / 250	3.8	− 3.3
Maintained at T_{amb}	Measured with two thermocouples (TC_{mid} position)	4.0 %	125 / 125	–	− 2.9
			250 / 125	–	− 2.8
			125 / 250	–	− 2.4
			250 / 250	–	− 2.3
		4.5 %	125 / 125	–	− 3.3
			250 / 125	–	− 3.1

			125 / 250	–	− 2.6
			250 / 250	–	− 2.6
	Measured with two thermocouples (TC_{side} position)	4.0 %	125 / 125	–	− 2.8
			250 / 125	–	− 2.7
			125 / 250	–	− 2.3
			250 / 250	–	− 2.2
		4.5 %	125 / 125	–	− 3.2
			250 / 125	–	− 3.0
			125 / 250	–	− 2.6
			250 / 250	–	− 2.5

Reviewer 2's comments

This manuscript presents the first thin-film-based heat-driven elastocaloric cooling system, wherein thermal energy actuates a shape memory alloy (SMA) to induce elastocaloric cooling. The authors report a temperature span of 12.9 K at the refrigerant film level and 4.0 K at the device level under an 86 °C heat input, alongside a specific cooling power of 5.49 W g^{-1} and a coefficient of performance (COP) of 4.02. While the overarching concept of heat-driven elastocaloric cooling is both important and promising, the claimed novelties are undermined by three critical issues that limit the manuscript's significance.

We sincerely thank the Reviewer for the careful evaluation of our manuscript and for the constructive and detailed comments. We appreciate the recognition of the importance and potential of heat-driven elastocaloric cooling, as well as the critical perspective regarding the manuscript's positioning and significance. We have carefully considered each of the points raised and have revised the manuscript accordingly. Below, we respond to each comment in detail.

Comment 1: *The concept is not new. The authors repeatedly describe their actuation method as novel. However, the use of SMA as a thermal actuator for elastocaloric cooling has been previously introduced, e.g., ref. [26]. The thin-film geometry is indeed a new implementation, but its selection appears suboptimal. The slow thermal response of the heat actuator (<1 Hz, Fig. 4b) is incompatible with the high-frequency potential of microfilm-based cooling. For instance, TiNiFe films have demonstrated ~19 W g^{-1} specific cooling power at 4 Hz when driven by an electric motor as authors showed in ref. [16]. Without leveraging the frequency advantage, the thin-film configuration suffers from increased heat leakage, which diminishes its practical utility.*

Response: We thank the Reviewer for this important and thoughtful comment.

We agree that the general concept of heat-driven elastocaloric cooling has been previously proposed, particularly in Ref. [26], where a regenerative architecture was introduced based on thermodynamic modeling and numerical simulations at macroscopic scale. In response to the Reviewer's and Editor's comments, we have removed all priority-based wording (e.g., "novel", "new", "first") and clarified the positioning of our work. The contribution of the present study lies not in proposing the concept itself, but in experimentally realizing thermally powered shape-memory actuation directly coupled to a thin-film elastocaloric refrigerant architecture at miniature scale, with integrated device-level validation. This distinction is now explicitly clarified in the Introduction to avoid any implication of conceptual precedence.

Regarding the operating frequency, we agree that thin-film refrigerants can achieve significantly higher specific cooling power when driven by high-speed electromechanical actuators, as demonstrated in Ref. [16]. However, the present work addresses a fundamentally different actuation paradigm. In heat-driven systems, the governing limitation is thermal transport within the actuator rather than mechanical inertia. The achievable strain rate and operating frequency are therefore intrinsically constrained by heating and cooling time constants of the actuator film. This thermally limited regime applies to heat-driven elastocaloric systems in general and is not specific to the thin-film geometry used here.

We agree that lower operating frequency increases parasitic heat dissipation during non-contact intervals, which reduces the device-level temperature span. This limitation is now explicitly discussed in the revised manuscript. Importantly, this challenge reflects the central engineering barrier for heat-driven elastocaloric cooling more broadly: enhancing actuator thermal response to increase strain rate and cycling frequency. We have therefore added discussion outlining potential strategies, including optimized actuator geometry, enhanced heat transfer, and alternative thermally driven actuation mechanisms such as bistable, agonist–antagonist, or catch-and-release designs.

The present work establishes the experimental feasibility of thin-film heat-driven elastocaloric integration and identifies actuator thermal dynamics as the key parameter governing future performance scaling. Improving strain rate under purely thermal driving represents a general research direction for heat-driven elastocaloric systems.

Changes made:

- Removed all priority-based wording (e.g., "new", "novel", "first") throughout the manuscript, including the *Abstract*, *Introduction*, *Results*, and *Conclusion*.
- Added a paragraph in the *Introduction* (Page 2, Line 77–84) explicitly clarifying the distinction from Ref. [26]:

"A regenerative heat-driven elastocaloric concept has previously been proposed through thermodynamic modeling and numerical simulations at macroscopic scale[26], providing important theoretical insights into cycle design and energy flow. In contrast, the present work experimentally realizes thermally powered shape-memory actuation directly coupled to a thin-film elastocaloric refrigerant architecture at miniature scale. The integrated prototype achieves a 12.9 K temperature span at the material level and a 4.0 K temperature span at the device level under Joule-heated thermal actuation at 86 °C, providing an experimental demonstration of film-based heat-driven elastocaloric cooling.".

- Added discussion in the *Methods* section (Page 10, Line 439–453) addressing frequency limitation and potential strategies for improving actuator response:

"In both cases, the limitation originates from thermally constrained actuation dynamics, which restrict both the strain rate and the achievable operating frequency. Fully adiabatic conditions typically require strain rates $\geq 0.1\ s^{-1}$ ($\approx 750\ \mu m/s$), whereas the present actuator provides $0.09\ s^{-1}$ during loading ($\approx 639\ \mu m/s$) and $0.07\ s^{-1}$ during unloading ($\approx 526\ \mu m/s$). These sub-adiabatic strain rates allow partial heat exchange during phase transformation. At the device level, the temperature span is further limited by finite heat-transfer rates between the refrigerant film and the heat sink/source, as well as the thermal mass of the heat exchangers during cyclic operation. In the absence of regenerative or cascaded architecture[15,45], the net temperature lift accumulated per cycle remains lower than the intrinsic material temperature change. Future improvements may focus on increasing strain rates through optimized actuator geometry, enhanced heat transfer, or alternative actuation strategies to more fully exploit the intrinsic cooling potential of the refrigerant film. Advanced actuation concepts, including bistable configurations, agonist–antagonist designs, or catch-and-release mechanisms[46,47], together with multistage cascading architectures on the cooling side[15,45], may further enhance the effective device-level temperature span.".

Reference:

[46] Chen, X., Bumke, L., Quandt, E. & Kohl, M. Bistable Actuation Based on Antagonistic Buckling SMA Beams. *Actuators* **12**, 422 (2023).

[47] Bevilacqua, D. *et al.* Performance analysis of agonist-antagonist SMA micro-wires and resonant compliant joint in bio-inspired bat-like flapping wings. in *Bioinspiration, Biomimetics, and Bioreplication XIV* vol. 12944 33–42 (SPIE, 2024).

Comment 2: *Exaggerated performance metrics. Key performance indicators, including cooling power, COP, and exergy efficiency, are incorrectly measured or calculated. The calculated cooling power only showed the microfilm TiNiFe provided ~3 mW cooling to the heat source, which balanced its own internal energy change during the initial cooling stage and heat leak to the ambient during the equilibrium state, yielding no net cooling from the heat source. From a system-level perspective, the effective cooling power should be considered zero, consistent with standard practice in the field.*

Response: We thank the Reviewer for this important comment regarding the definition and measurement of cooling power.

We respectfully clarify that the cooling power reported in the manuscript corresponds to the standard definition used in elastocaloric cooling studies under zero temperature lift conditions, where the instantaneous cooling capacity is evaluated from the initial temperature slope of the heat source before a temperature gradient is established (temperature-slope method). This approach has been widely adopted in film- and foil-based elastocaloric systems (Refs. [18, 48]) to quantify intrinsic cooling capacity independent of steady-state heat leakage.

Specifically, the temperature-slope calculated cooling power (3.08 mW for the Joule-heated configuration) is derived from:

$$\dot{Q}_{\mathrm{c}} = m_{\mathrm{source}} c_{\mathrm{p,source}} \dot{T}_{\mathrm{source}}$$

evaluated during the first cooling cycle at zero temperature span, where backflow heat leakage is negligible. Under this condition, the measured temperature slope reflects the net heat extracted from the heat source by the refrigerant film. This definition does not correspond to steady-state equilibrium, where the net cooling power indeed approaches zero due to balance with environmental heat leak.

Nevertheless, we agree that direct experimental validation strengthens the reliability of the reported values. Therefore, following the Reviewer's suggestion, we have implemented an independent counter-heating measurement method, in which a calibrated 0.5 Ω NiCr resistance wire supplies electrical power to the heat source to balance the cooling effect. The direct counter-heating measured cooling power at zero temperature lift is 2.79 mW, which is in close agreement with the temperature-slope calculated value of 3.08 mW (Supplementary Fig. 7 and Supplementary Table 3). The small deviation (<10%) is attributed to additional thermal leakage during counter-heating operation. Importantly, we do not claim net cooling under steady-state temperature lift without compensation. As shown in Supplementary Table 3, the cooling power decreases with increasing temperature lift and approaches zero at finite temperature difference, consistent with thermodynamic expectations.

To avoid ambiguity, we have:

- Added direct counter-heating measurements of cooling power to experimentally validate the temperature-slope method.
- Explicitly clarified that reported cooling power values correspond to zero temperature lift conditions, where intrinsic cooling capacity is evaluated.
- Revised COP and exergetic efficiency calculations under multiple input-power bases and cooling-power determination methods, with all evaluation conditions systematically summarized.

Reference:

[18] Bruederlin, F., Ossmer, H., Wendler, F., Miyazaki, S. & Kohl, M. SMA foil-based elastocaloric cooling: from material behavior to device engineering. *J. Phys. D: Appl. Phys.* **50**, 424003 (2017).

[48] Ludwig, C., Leutner, J., Prucker, O., Ruehe, J. & Kohl, M. Natural Rubber Foil-Based Elastocaloric Cooling. in *ACTUATOR 2024; International Conference and Exhibition on New Actuator Systems and Applications* 132–135 (2024).

Changes made:

- Clarified in the revised manuscript that the temperature-slope calculated cooling power is determined from the initial temperature slope of the heat source under zero temperature lift conditions, consistent with established methodology for film-based elastocaloric systems.
- Added direct counter-heating measurements of cooling power to provide an independent experimental validation (*Supplementary Fig. 7* and *Supplementary Table 3*).

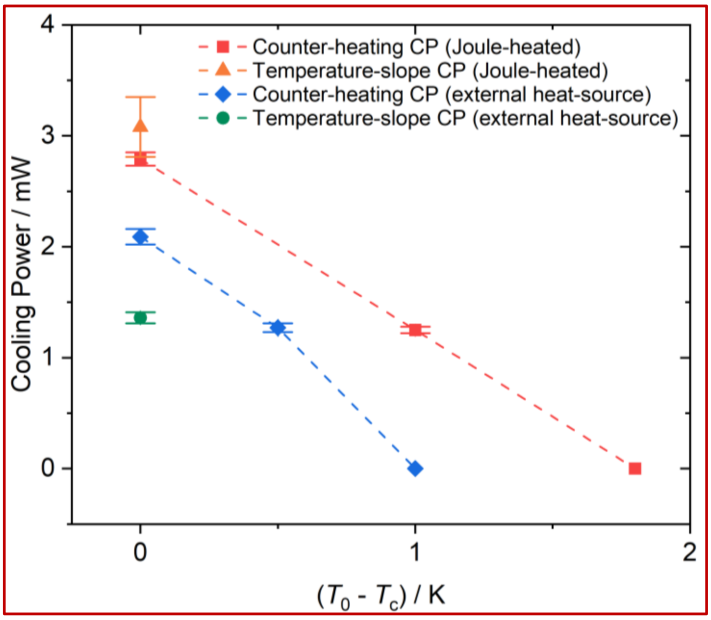

Supplementary Fig. 7. Cooling power under different actuation modes and determination methods. Cooling power values for the Joule-heated actuation configuration are shown in red (counter-heating method) and orange (temperature-slope method). Cooling power values for the external heat-source actuation configuration are shown in blue (counter-heating method) and green (temperature-slope method). Cooling power determined using the temperature-slope method is derived from the initial temperature decay rate of the heat source during the first cooling cycle at zero temperature lift. Cooling power determined using the counter-heating method is obtained by supplying electrical power through a calibrated resistance wire to offset the cooling effect. The parameters used in the temperature-slope analysis are listed in Supplementary Table 2, and detailed numerical values of cooling power are provided in Supplementary Table 3. Data are presented as mean ± standard deviation (n = 3 independent experiments). Symbols represent experimental data points, and dashed lines serve as guides to the eye.

Supplementary Table 3. Cooling power of Joule-heated and externally heat-driven elastocaloric systems determined by temperature-slope calculation and direct counter-heating measurement.

Actuation mode	$T_0 - T_c$ (K)	Cooling power (temperature-slope) (mW)	Cooling power (counter-heating) (mW)
Joule-heated actuation	0	3.08	2.79
	1	–	1.25
	2	–	0
External heat-source actuation	0	1.36	2.09
	0.5	–	1.27
	1	–	0

Cooling power determined using the temperature-slope method is derived from the initial temperature decay rate of the heat source under zero temperature lift conditions. Accordingly, values from the temperature-slope method are only provided for $T_0 - T_c = 0$ K. Cooling power determined using the counter-heating method is obtained as described in the Methods section. "–" indicates not applicable.

- Comparison between temperature-slope calculated and directly measured cooling power has been added to the *Methods* section (Page 10, Line 454–463):

"Cooling power was determined using both the temperature-slope method and direct counter-heating measurement. At zero temperature lift, the cooling powers obtained from the temperature-slope method and the counter-heating method are 3.08 and 2.79 mW, respectively (Supplementary Fig. 7 and Supplementary Table 3). The close agreement between these values supports the reliability of the cooling power evaluation. The slightly lower value obtained from the counter-heating method is attributed to additional thermal leakage to the surroundings under finite temperature-span conditions during counter-heating operation. The coefficients of performance (COP) at zero temperature lift and exergetic efficiency at −1.0 K temperature drop, derived using cooling power from both methods under different input-power definitions, are summarized in Supplementary Table 4."

- The acquisition methods for cooling power have been clarified in the *Methods* section (Page 11, Line 491–497):

"Cooling power (CP) and specific cooling power (SCP) were determined using two independent approaches: the temperature-slope method and a direct counter-heating measurement. In the temperature-slope method, cooling power is obtained from the initial temperature decay rate of the heat source during the first cooling cycle at zero temperature lift[18,48]. In the counter-heating method, a calibrated 0.5 Ω NiCr resistance wire is used to electrically supply heat to the heat source until thermal balance is reached, and the electrical input power required to offset the cooling effect is taken as the cooling power.".

- Performance values have been updated in the "*Coupled heat-driven system using Joule heating*" (Page 5, Line 212–214) and *Conclusion* (Page 7, Line 295) to reflect directly measured cooling power: "The cooling power (CP) at zero temperature lift, determined using the counter-heating method, is 2.79 mW, corresponding to a specific cooling power (SCP) of 5.24 W g^{-1}."

- Revised COP and exergetic efficiency calculations under multiple input-power bases and cooling-power determination methods, with all evaluation conditions systematically summarized in *Supplementary Table 4*.

Comment 3: *Furthermore, the COP is overstated, as it excludes the electrical input required to drive the heat source/sink. These omissions significantly weaken the claimed performance and novelty.*

Response: We thank the Reviewer for raising this important concern. We agree that a comprehensive system-level COP assessment should explicitly account for all relevant input powers, including electrical energy required for actuation and thermal control.

In the revised manuscript, we have therefore expanded the COP analysis to include multiple input-power definitions beyond the actuator thermal-input basis. Specifically, the revised evaluation now considers:

- Thermal energy absorbed by the actuator film (thermal input basis)
- Electrical power supplied for Joule heating of the actuator film (electrical input basis)
- Input power required to maintain the external heat-source temperature (electrical input basis)
- Electrical power consumption of the two auxiliary linear actuators used to cyclically move the heat exchangers (Full system + auxiliary actuators)

When these additional electrical inputs are included, the full-system COP decreases substantially compared to values calculated solely on the thermal input basis. For example, in the Joule-heated configuration:

- Full-system COP = 0.09 (thermal input basis)
- Full-system COP = 0.02 (electrical input basis)
- Full-system COP $\approx 7 \times 10^{-4}$ (including auxiliary actuator consumption)

Similar trends are observed for the externally heat-driven configuration.

We note that the present prototype employs high-precision laboratory servo actuators to enable flexible experimental control. These components consume significantly more electrical power than would be required in a purpose-designed compact system. Therefore, while the expanded analysis provides a transparent and comprehensive accounting of total input power, it reflects the prototyping hardware configuration rather than an optimized device architecture.

All definitions, formulations, and integration procedures for the different COP evaluation criteria are now provided in *Supplementary Note 3*, and a complete summary of results is presented in *Supplementary Table 4*.

Changes made:

- Expanded COP analysis to include (i) power consumption of the auxiliary linear actuators used to move the heat exchangers, (ii) electrical power supplied for Joule heating, and (iii) input power required to maintain the external heat source.
- Added expanded system-level COPs in *Supplementary Table 4*, summarizing all evaluation conditions, including cases where auxiliary actuator electrical consumption is considered.
- Added detailed mathematical formulations and power-integration procedures for each input-power basis in *Supplementary Note 3*, including explicit expressions for full-system evaluation with auxiliary actuator power consumption.

- Added clarification in *Supplementary Note 3* (Page 7): "In the present laboratory prototype, auxiliary actuator consumption accounts for more than 90% of the total electrical input power due to the use of high-precision servo actuators selected for experimental control. These values reflect the prototyping configuration rather than representing an intrinsic thermodynamic limitation of thermally driven elastocaloric cooling."

Supplementary Table 4. Coefficient of performance (COP) and exergetic efficiency of Joule-heated and externally heat-driven elastocaloric systems under different evaluation criteria. Definitions of COP and exergetic efficiency, including the corresponding input-power bases, are provided in Supplementary Note 3.

Evaluation conditions		COP	Exergetic efficiency
Joule heating actuation		evaluated at $T_c - T_0 = 0$ K	evaluated at $T_c - T_0 = -1$ K
Temperature-slope method	Cooler (with work recovery)	5.46	–
	Cooler (without work recovery)	2.88	–
	Thermal actuator efficiency (thermal input basis)	0.03	–
	Thermal actuator efficiency (electrical input basis)	0.01	–
	Full system (thermal input basis)	0.09	–
	Full system (electrical input basis)	0.02	–
	Full system (thermal input basis + auxiliary actuators)	0.0008	–
	Full system (electrical input basis + auxiliary actuators)	0.0007	–
Counter-heating method	Cooler (with work recovery)	4.94	4.21 %
	Cooler (without work recovery)	2.61	2.22 %
	Thermal actuator efficiency (thermal input basis)	0.03	3.27 %
	Thermal actuator efficiency (electrical input basis)	0.01	0.84 %
	Full system (thermal input basis)	0.09	0.07 %
	Full system (electrical input basis)	0.02	0.02 %
	Full system (thermal input basis + auxiliary actuators)	0.0007	0.001 %

	Full system (electrical input basis+ auxiliary actuators)	0.0007	0.001 %
External heat-source actuation		evaluated at $T_c - T_0 = 0$ K	evaluated at $T_c - T_0 = -0.5$ K
Temperature-slope method	Cooler (with work recovery)	2.31	–
	Cooler (without work recovery)	1.50	–
	Thermal actuator efficiency (electrical input basis)	0.0024	–
	Full system (electrical input basis)	0.0036	–
	Full system (electrical input basis+ auxiliary actuators)	0.0002	–
Counter-heating method	Cooler (with work recovery)	3.55	1.37 %
	Cooler without work recovery	2.31	0.89 %
	Thermal actuator efficiency (electrical input basis)	0.0024	0.24 %
	Full system (electrical input basis)	0.0056	0.002 %
	Full system (electrical input basis+ auxiliary actuators)	0.0003	< 0.001 %

Note:

- COP values reported for the full system correspond to the one-way shape memory actuator configuration without work recovery. Values labeled "with work recovery" represent a theoretical upper bound of the cooling unit and are provided for benchmarking future bidirectional actuator designs.
- For Joule-heated actuation, the full-system COP/exergetic efficiency on a thermal-input basis (including auxiliary actuators) and on an electrical-input basis (including auxiliary actuators) are identical (0.0007/0.001%). This equivalence arises from the dominant input power consumption of the auxiliary actuators combined with the relatively small cooling power measured via direct counter-heating.

Comment 4: *Inappropriate heat source representation. The authors justify their concept by referencing low-grade heat sources such as waste heat and solar thermal energy. However, the experimental setup relies on Joule heating within the actuator, which differs fundamentally in heat transfer behavior. Joule heating produces a parabolic temperature profile due to a uniform internal generation, whereas external heat sources yield linear profiles from boundary heating. This discrepancy becomes increasingly relevant when scaling the system, casting doubt on the validity of the actuator's performance and the broader applicability of the proposed concept.*

Response: We thank the Reviewer for this important and technically insightful comment. We agree that Joule heating (internal volumetric heat generation) and external heat-source heating (boundary-driven heat transfer) involve fundamentally different thermal transport mechanisms and may lead to different temperature profiles within the actuator film. This distinction is indeed relevant when considering scalability and practical implementation.

To directly address this concern, we have implemented and experimentally validated a configuration in which Joule heating is fully replaced by an external solid heat source in the actuation unit. In this modified setup, thermal energy is supplied via solid–solid contact between the actuator film and a temperature-controlled copper plate heated by an external microheater. This configuration eliminates internal Joule heating within the actuator and enables evaluation under boundary-driven heating conditions representative of practical low-grade heat sources. Under identical film dimensions and operating frequency (0.83 Hz), the externally heat-driven system achieves:

- A device-level temperature span of 2.2 K
- A cooling power of 1.36 mW (temperature-slope method) and 2.09 mW (counter-heating method)
- A specific cooling power of 3.92 W g^{-1}

Although the performance is lower than in the Joule-heated configuration (4.0 K span), this reduction is primarily attributed to thermally constrained strain rates and the shorter achievable stroke under the present actuator geometry. Importantly, the results confirm that elastocaloric cooling can be driven purely by externally supplied thermal energy under boundary-heating conditions, thereby validating the broader applicability of the heat-driven concept.

We have added a dedicated section in the main text and Methods describing the externally heat-driven configuration, along with new figures and supplementary data detailing device architecture, actuation dynamics, and performance metrics. The distinction between Joule-heated and externally heat-driven operation is now clearly presented throughout the manuscript.

Changes made:

- Implemented and experimentally validated an externally heat-driven configuration using solid-to-solid thermal contact instead of internal Joule heating (new *Fig. 5* and related discussion).
- Added a new section "*Coupled heat-driven system using an external heat source*" (Page 6, Line 240–267) in the main text describing device design, operating parameters, and performance under external heat-source actuation.
- Added a new *Methods* subsection (Page 11, Line 464–485) detailing construction and operation of the externally heat-driven actuation unit.
- Added *Supplementary Figs. 6, 9*, and *15* to document boundary-heating configuration, actuation dynamics, and working principle.
- Updated *Supplementary Fig. 7, Supplementary Tables 3* and *Supplementary Tables 4* to include cooling power, COP, and exergetic efficiency values for externally heat-driven operation.
- Revised *Abstract*, *Results*, and *Conclusion* to clearly distinguish between externally heat-driven configurations and Joule-heated.

For clarity, the **selected** key newly added figures and corresponding text passages are provided below:

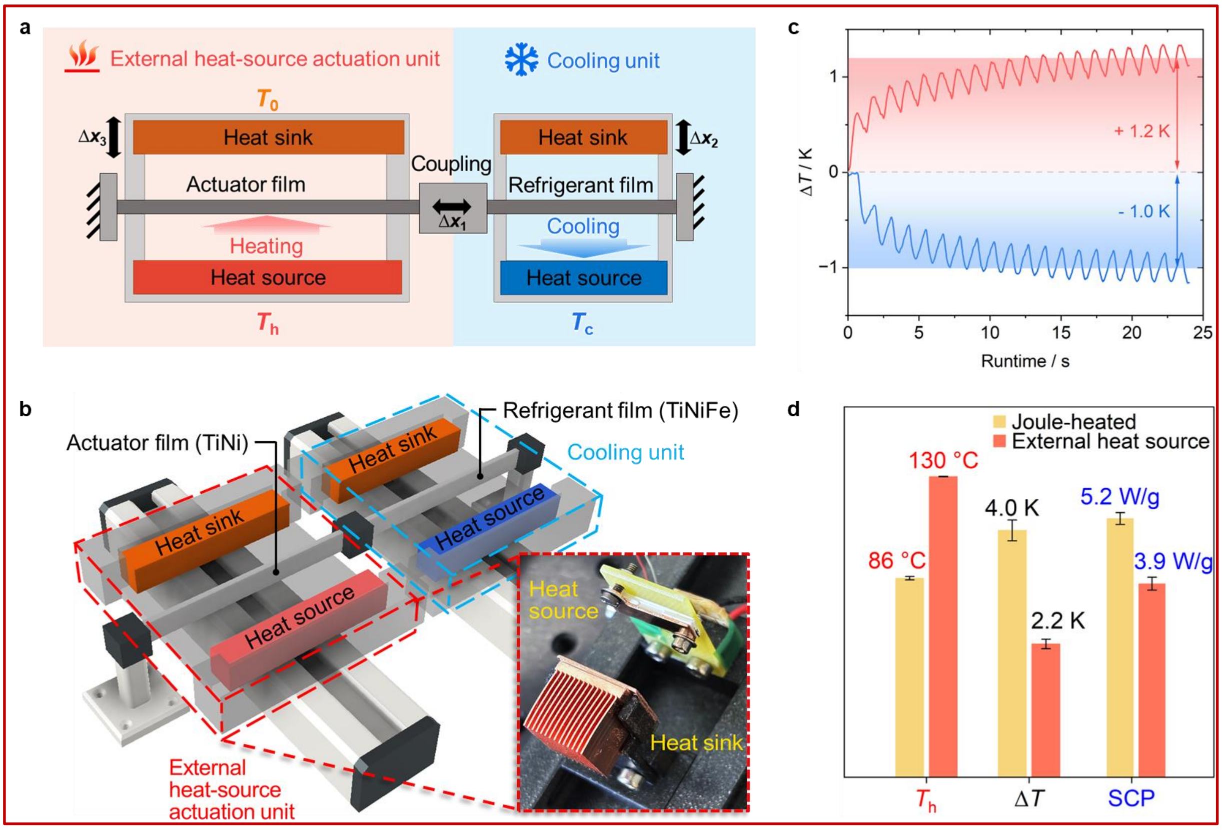

Fig. 5: System design and performance of the elastocaloric cooling device under external heat-source actuation. a, Schematic illustration of the device architecture, where Joule heating is replaced by an external solid heat source in the actuation unit, enabling thermal energy input through solid-to-solid contact. T_c, T_h, and T_0 denote the cooling temperature in the cooling unit, the heating temperature in the actuation unit, and the ambient temperature, respectively. **b**, Three-dimensional representation of the prototype showing the actuator film, refrigerant film, external heat source in the actuation unit, and the heat exchangers. Inset: close-up view of the fin-structured heat sink and the heat source assembly in the actuation unit. The heat source consists of a platinum microheater bonded to a thin Cu contact plate that interfaces with the actuator film. **c,** Device-level temperature span (ΔT) over 24 s of operation. After 20 cycles, a steady-state temperature span of 2.2 K is reached, corresponding to an average temperature rise of +1.2 K at the hot side and an average temperature drop of −1.0 K at the cold side. **d,** Comparison of heating temperature T_h, temperature span (ΔT), and specific cooling power (SCP, counter-heating method) between Joule-heated actuation and external heat-source actuation. The proof-of-concept external heat-source configuration exhibits lower performance primarily due to the reduced actuation stroke under the current geometric constraints. Data are shown as mean ± standard deviation (n = 3 independent experiments).

New section “*Coupled heat-driven system using an external heat source*” in the Main text (Page 6, Line 240–267):

“To verify true heat-driven operation, Joule heating was replaced with an external solid heat source in the actuation unit, enabling direct conductive heating of the actuator film (Fig. 5a, b). The verification prototype was operated using the same film dimensions and cycling frequency as the Joule-heated configuration to allow direct comparison. The external heat source was maintained at 130 °C (T_h) to provide sufficient thermal input for uniaxial loading of the refrigerant film by approximately 300 μm within a 0.25 s heating interval (Supplementary Fig. 9a). Active motion control of the heat source and heat sink in the actuation unit constrained the loading and unloading durations to approximately 0.6 s (Supplementary Fig. 9b, c), corresponding to strain rates between 0.053 s^{-1} to 0.066 s^{-1} (Supplementary Fig. 9d).

Cooling performance was evaluated under these conditions, with the heating time increased to 0.35 s to ensure sufficient thermal input in the coupled heat-driven system using an external heat source. With a slightly reduced stroke (strain ≈ 4.1%), the externally heat-driven device achieves a steady-state temperature span of 2.2 K at the same operating frequency as the Joule-heated coupled system (Fig. 5c, d). The cooling power at zero temperature lift, determined using the counter-heating method, is 2.09 mW, corresponding to a specific cooling power of 3.92 W g^{-1} (Supplementary Fig. 7 and Supplementary Table 3). When the heat sink in the cooling unit is maintained near ambient temperature, the cold-side temperature drop ($T_c - T_0$) increases from −1.0 K to −1.4 K (Supplementary Fig. 6b).

Compared to the Joule-heated configuration, the externally heat-driven system exhibits reductions of 1.8 K in temperature span and 1.32 W g^{-1} in specific cooling power (Fig. 5d), primarily due to the lower achievable stroke under the present actuator geometry. The higher required heating temperature of 130 °C, compared to 86 °C in the Joule-heated case, reflects the different heat-transfer mechanisms involved. Joule heating generates volumetric internal heat, whereas the external heat source relies on boundary-driven conduction. Optimization of actuator geometry and transformation temperature A_f, together with improved heat-transfer design, may reduce the required heat source temperature and enhance actuation efficiency in future implementations.”.

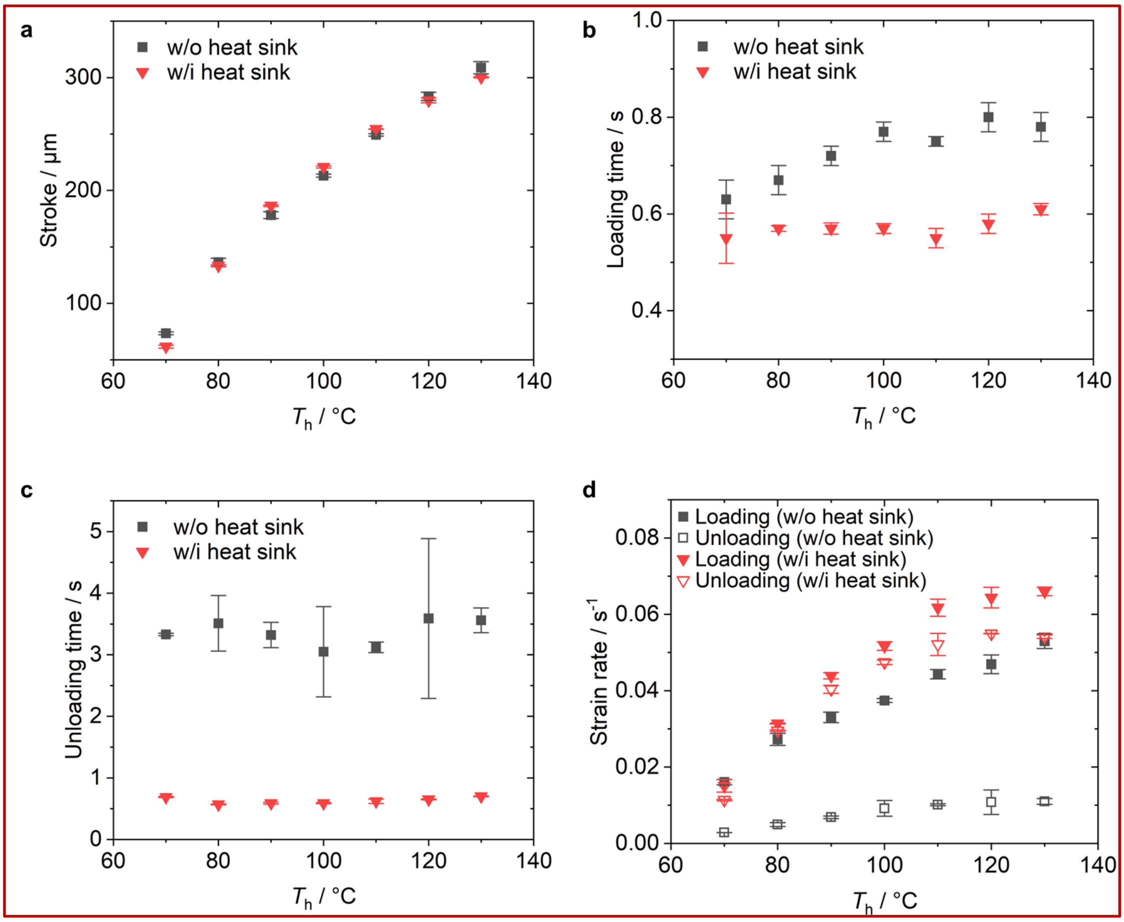

Supplementary Fig. 9. Performance of the external heat-source actuation unit at heat-source temperatures from 70 to 130 °C with a 250 ms contact time. Data obtained without and with implementation of the heat sink are shown in black and red, respectively. **a,** Actuation stroke as a function of heat-source temperature (T_h). At 130 °C, strokes exceed 300 µm for both configurations, providing sufficient strain to load the refrigerant film. **b,** Loading time versus T_h. Without active heat-sink implementation, loading times range from approximately 0.6 to 0.8 s. Incorporating active heat-sink movement reduces the loading time to 0.6 s and improves consistency. **c,** Unloading time versus T_h. Without active heat-sink control, unloading exceeds 3 s and shows significant variability due to uncontrolled convective cooling of the actuator film. With active heat-sink implementation, unloading time is constrained to 0.6 s, markedly improving repeatability. **d,** Corresponding strain rates during loading and unloading. Active heat-sink control increases both loading and unloading strain rates, approaching the adiabatic regime, reaching 0.07 s^{-1} (loading) and 0.05 s^{-1} (unloading) at 130 °C. Data are shown as mean ± standard deviation (n = 3 independent experiments).

Supplementary Table 3. Cooling power of Joule-heated and externally heat-driven elastocaloric systems determined by temperature-slope calculation and direct counter-heating measurement.

Actuation mode	$T_0 - T_c$ (K)	Cooling power (temperature-slope) (mW)	Cooling power (counter-heating) (mW)
Joule-heated actuation	0	3.08	2.79
	1	–	1.25
	2	–	0
External heat-source actuation	0	1.36	2.09
	0.5	–	1.27
	1	–	0

Cooling power determined using the temperature-slope method is derived from the initial temperature decay rate of the heat source under zero temperature lift conditions. Accordingly, values from the temperature-slope method are only provided for $T_0 - T_c$ = 0 K. Cooling power determined using the counter-heating method is obtained as described in the Methods section. "–" indicates not applicable.

New section in the *Methods* (Page 11, Line 464–485):

"The external heat source was fabricated in-house using a 5 × 5 mm^2 platinum microheater (Innovative Sensor Technology). The microheater was bonded with thermally conductive adhesive to a 0.6 mm-thick Cu plate, which served as the contact interface with the actuator film. A thermocouple was attached to the Cu plate for closed-loop PID temperature control. A fin-structured Cu heat sink was employed to remove heat from the actuator film during the cooling stage.

The heat-source temperature was varied between 70 and 130 °C with a 250 ms contact time to determine the required heating temperature, T_h, for achieving sufficient loading stroke and acceptable loading/unloading times (Supplementary Fig. 9). The device operates in a four-step cycle, as illustrated in Supplementary Fig. 15. The operating frequency was set to 0.83 Hz, identical to that of the Joule-heated configuration for direct comparison. The loading and unloading velocities were 507 μm/s (stain rate 0.07 s^{-1}) and 511 μm/s (stain rate 0.07 s^{-1}), respectively.

Cooling power was determined using both the temperature-slope method and the direct counter-heating method. At zero temperature lift, the cooling powers obtained from the temperature-slope method and the counter-heating method are 1.36 mW and 2.09 mW, respectively (Supplementary Fig. 7 and Supplementary Table 3). The slightly higher value obtained from the counter-heating method may reflect increased sensitivity to ambient disturbances at low power levels, whereas the temperature-slope method may underestimate cooling power due to unaccounted thermal mass in surrounding components. COP values at zero temperature lift and exergetic efficiency at a −0.5 K temperature drop, evaluated under different input-power definitions, are summarized in Supplementary Table 4.

Comment 5: *The statement "Loading times are limited to ~500 ms and showed little improvement with higher currents or longer pulses" is insufficiently supported. Only data for 0.9 A and 1 A are shown in Supplementary Fig. 3a. A comprehensive dataset is needed to substantiate this claim.*

Response: We thank the Reviewer for highlighting this point. We agree that the original wording could be interpreted as implying a broader current range than what was experimentally investigated.

In the present study, loading-time measurements were performed primarily at a Joule heating current of 1.0 A while varying the pulse duration. Experiments with substantially higher currents were intentionally not conducted to avoid overheating of the actuator film and polymer clamping structures. In addition, increasing heating power would lead to greater heat accumulation in the actuator film, which is unfavorable for the subsequent cooling and unloading stage and would prolong cycle time. For these reasons, the operating range was constrained to ensure stable and reproducible cyclic operation.

We have revised the manuscript to accurately reflect the tested conditions and removed the broader claim regarding current dependence.

Changes made:

- The description of loading-time behavior has been revised in the main text (Page 4, Line 166–168) to explicitly state the tested condition: "Loading times remain above 500 ms and show no clear dependence on pulse duration at a Joule heating current of 1.0 A (Supplementary Fig. 3a)."
- The rationale for not testing higher currents or longer pulse durations has been clarified in the *Methods* (Page 9, Line 378–381): "Higher heating currents and longer pulse durations were not tested to prevent overheating of the actuator film and polymer clamping structures, and to avoid excessive heat accumulation that would prolong the subsequent cooling stage."

Comment 6: *The manuscript lacks an uncertainty analysis. Quantitative uncertainties for temperature, cooling power, and COP should be provided.*

Response: We thank the Reviewer for emphasizing the importance of uncertainty analysis. Following this suggestion, we have systematically incorporated quantitative uncertainty reporting throughout the manuscript.

Specifically, error bars representing mean ± standard deviation (n = 3 independent experiments) have been added to key performance figures, including temperature span, cooling power, and COP. The corresponding numerical values are provided in the Supplementary Information to ensure full transparency.

Changes made:

- Added error bars (mean ± standard deviation, $n = 3$) to *Fig. 3d* for temperature-span measurements.
- Revised *Fig. 4d* to clearly display the existing COP uncertainty bars.
- Added uncertainty reporting in *Supplementary Fig. 7* for cooling power determined by both the temperature-slope and counter-heating methods.

- Included uncertainty analysis in *Supplementary Figs.* 4, *9*, and *13*.
- Provided detailed numerical values in *Supplementary Table 1* and *Supplementary Table 3*.

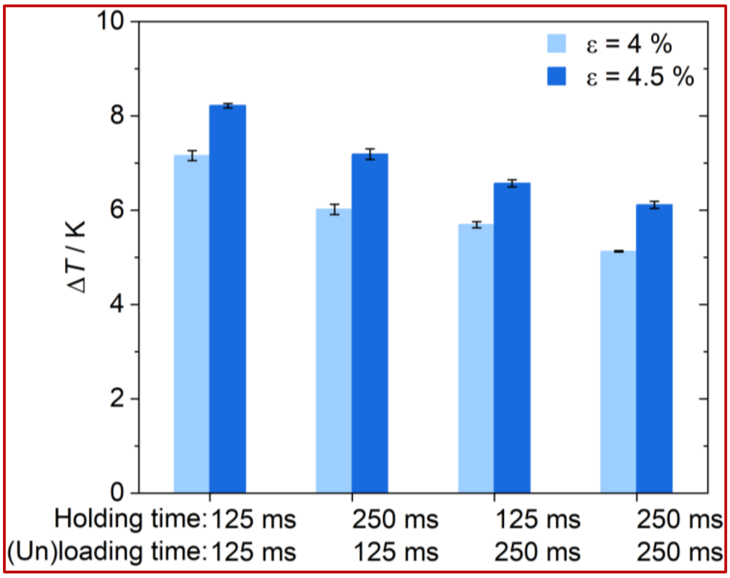

Fig. 3. Illustration and performance of the thermal actuation unit and elastocaloric cooling unit. … **d**, Device-level temperature span (ΔT) of the stand-alone cooling unit under imposed strains of 4% and 4.5%, tested at different (un)loading times (125–250 ms) and holding times (125–250 ms). The maximum temperature span ΔT is 8.2 K at 4.5% strain at 125 ms (un)loading and 125 ms holding time. Detailed values are given in Supplementary Table 1. Data are shown as mean ± standard deviation (n = 3 independent experiments).

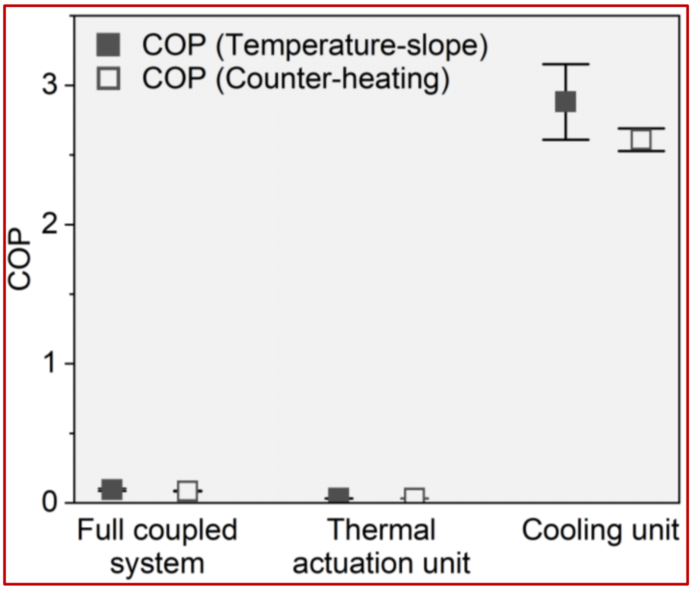

Fig. 4. Performance of the coupled heat-driven elastocaloric system under Joule-heated actuation. … **d**, Coefficient of performance at zero temperature lift (ΔT = 0 K) under different evaluation criteria. For the full system shown in this panel (Joule-heated actuation), COP is evaluated on a thermal input basis, where the thermal energy absorbed by the actuator film during each cycle is taken as the input power. The thermal actuator efficiency is defined as the ratio of its mechanical work output (without work recovery, WR) to the corresponding Joule-heating thermal input. All COP values shown are calculated without work recovery, consistent with the one-way SMA actuator configuration of the present prototype. Hollow symbols represent values obtained from the counter-heating method, while solid symbols represent values obtained from

the temperature-slope method. Detailed COP values are provided in Supplementary Table 4. The corresponding exergetic efficiencies and full efficiency definitions are given in Supplementary Note 3 and Supplementary Table 4. Data are shown as mean ± standard deviation (n = 3 independent experiments).

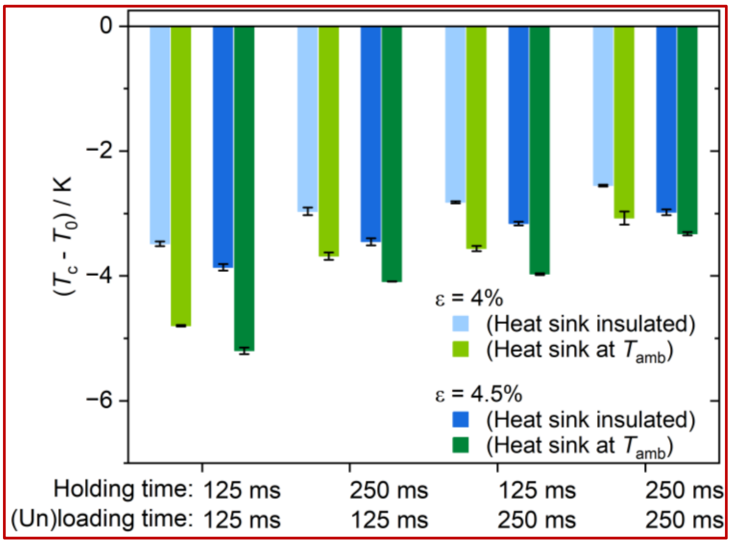

Supplementary Fig. 4. Comparison of temperature drop (T_c – T_0) under different heat-sink boundary conditions and strain ε. Temperature drops were measured using the stand-alone cooling unit driven by electromechanical actuators. Results are shown for ε = 4% and ε = 4.5% at different (un)loading and holding times (125 ms and 250 ms). Light blue and dark blue bars represent ε = 4% and ε = 4.5%, respectively, with the heat sink insulated. Light green and dark green bars represent ε = 4% and ε = 4.5%, respectively, with the heat sink maintained at ambient temperature (T_{amb}). Maintaining the heat sink near ambient temperature using a larger thermal mass (limiting the hot-side temperature rise to <1 K above ambient) increases the temperature drop by an average of 0.8 K compared to the insulated condition. Detailed numerical values are provided in Supplementary Table 1. Data are shown as mean ± standard deviation (n = 3 independent experiments).

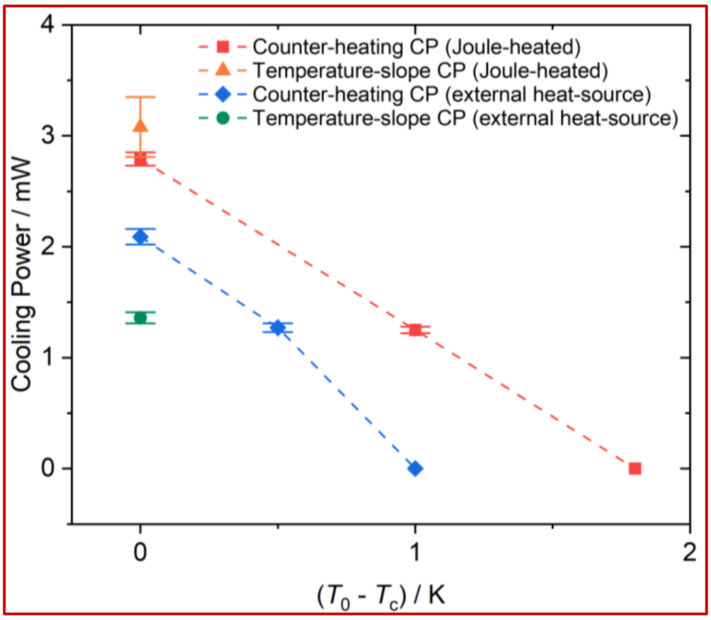

Supplementary Fig. 7. Cooling power under different actuation modes and determination methods. Cooling power values for the Joule-heated actuation configuration are shown in red (counter-heating method) and orange (temperature-slope method). Cooling power values for the external heat-source actuation configuration are shown in blue (counter-heating method) and green (temperature-slope method). Cooling power determined using the temperature-slope method is derived from the initial temperature decay rate of the heat source during the first cooling cycle at zero temperature lift. Cooling power determined using the counter-heating method is obtained by supplying electrical power through a calibrated resistance wire to offset the cooling effect. The parameters used in the temperature-slope analysis are listed in Supplementary Table 2, and detailed numerical values of cooling power are provided in Supplementary Table 3. Data are presented as mean ± standard deviation (*n* = 3 independent experiments). Symbols represent experimental data points, and dashed lines serve as guides to the eye.

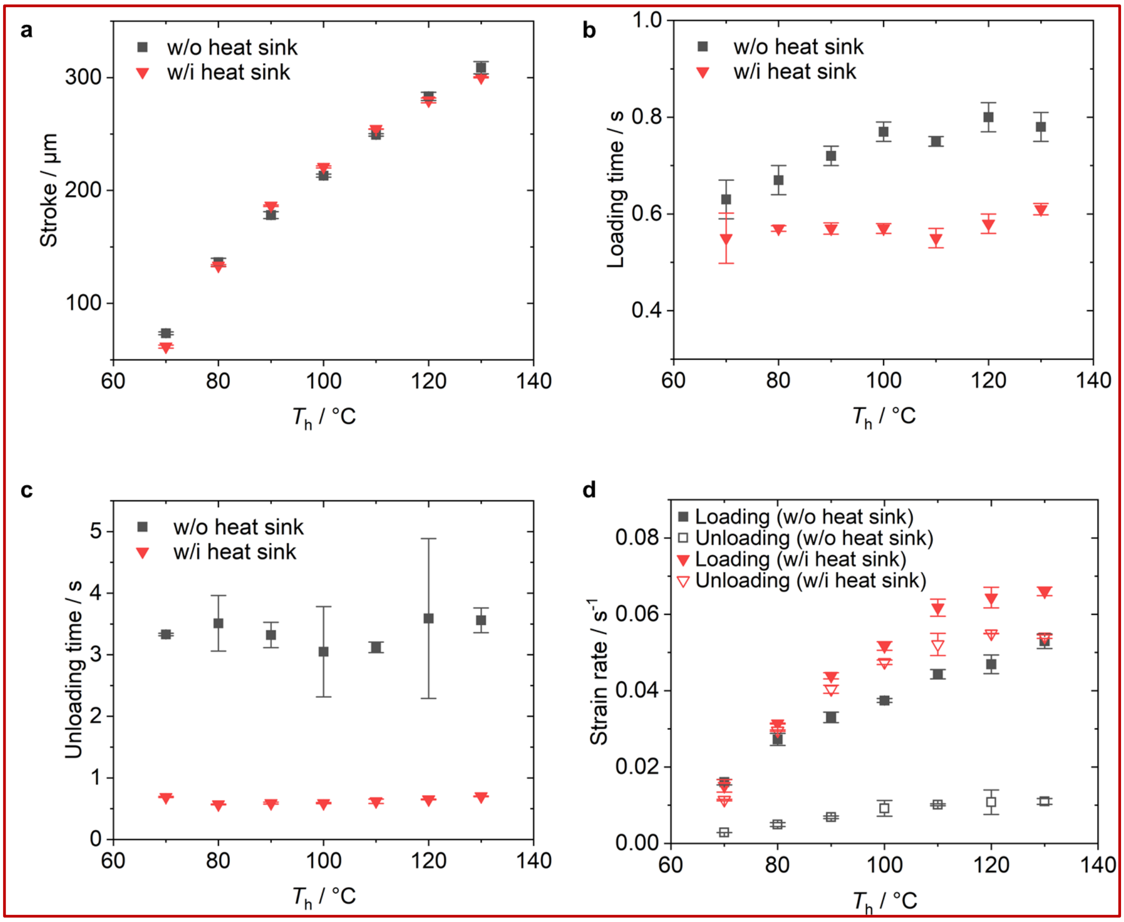

Supplementary Fig. 9. Performance of the external heat-source actuation unit at heat-source temperatures from 70 to 130 °C with a 250 ms contact time. Data obtained without and with implementation of the heat sink are shown in black and red, respectively. **a,** Actuation stroke as a function of heat-source temperature (T_h). At 130 °C, strokes exceed 300 μm for both configurations, providing sufficient strain to load the refrigerant film. **b,** Loading time versus T_h. Without active heat-sink implementation, loading times range from approximately 0.6 to 0.8 s. Incorporating active heat-sink movement reduces the loading time to 0.6 s and improves consistency. **c,** Unloading time versus T_h. Without active heat-sink control, unloading exceeds 3 s and shows significant variability due to uncontrolled convective cooling of the actuator film. With active heat-sink implementation, unloading time is constrained to 0.6 s, markedly improving repeatability. **d,** Corresponding strain rates during loading and unloading. Active heat-sink control increases both loading and unloading strain rates, approaching the adiabatic regime, reaching 0.07 s^{-1} (loading) and 0.05 s^{-1} (unloading) at 130 °C. Data are shown as mean ± standard deviation (*n* = 3 independent experiments).

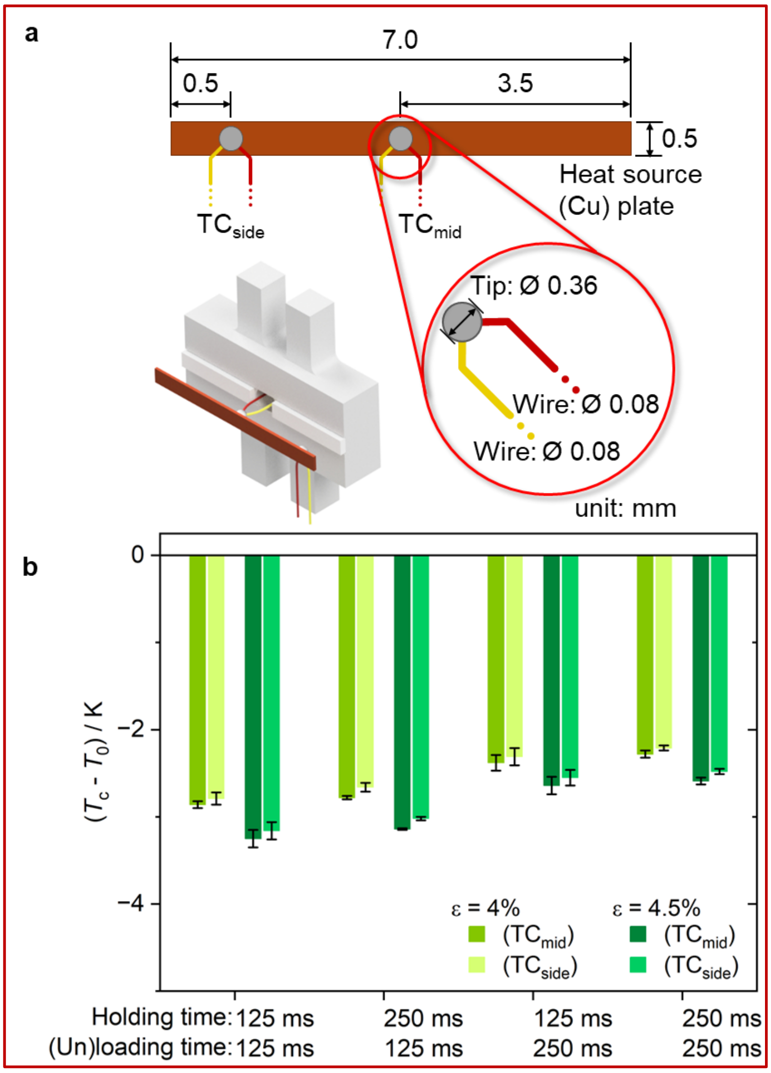

Supplementary Fig. 13. Validation of thermocouple measurement positions at the heat source in the cooling unit. a, Schematic illustration of the heat-source geometry (dimensions in mm) and thermocouple measurement locations. All device-level temperatures reported in the cooling unit are measured at the center of the heat source (TC$_{mid}$). An additional thermocouple (TC$_{side}$) was positioned near the edge of the heat source to verify spatial temperature uniformity. **b,** Comparison of temperature differences ($T_c - T_0$) measured at TC$_{mid}$ and TC$_{side}$ under 4% and 4.5% strain conditions using electromechanical actuation. The temperature difference between the two measurement positions remains below 0.1 K for all tested conditions, confirming a homogeneous temperature distribution across the heat source and validating the use of TC$_{mid}$ as a representative measurement point. Detailed numerical values are provided in Supplementary Table 1. Data are presented as mean ± standard deviation (n = 3 independent experiments).

Comment 7: *The use of a one-way SMA actuator prevents recovery of unloading work from the superelastic film. The authors should either revise the COP calculation to exclude work recovery or demonstrate a two-way SMA configuration.*

Response: We thank the Reviewer for this important comment. We agree that the present prototype employs a one-way shape-memory actuator and therefore does not recover mechanical work during unloading of the superelastic refrigerant film.

To ensure thermodynamic consistency, all system-level COP values and actuator efficiencies reported for the present device are calculated without work recovery in the main text, as shown in *Figure 4d*. These values represent the physically realizable performance of the current configuration. For completeness, COP values of the cooling unit with work recovery are retained only in Supplementary Table 4 as a theoretical upper bound for benchmarking future bidirectional actuator designs. They are not used in the evaluation or discussion of the present system-level performance.

We have revised the manuscript to make this distinction explicit and to ensure that the primary performance statements reflect the non-work-recovery configuration.

Changes made:

- Clarified throughout the main manuscript that all system-level COP and actuator-efficiency values are calculated without work recovery, consistent with the one-way SMA actuator configuration.
- Revised the COP calculations in the main text to exclude work recovery (e.g., *Fig. 4d*).
- Updated *Fig. 4d* and its caption to explicitly state that all COP values shown are calculated without work recovery: "All COP values shown are calculated without work recovery, consistent with the one-way SMA actuator configuration of the present prototype."
- Added an explicit clarification in *Supplementary Note 3* stating that: "In the present prototype, work recovery is not implemented due to the one-way SMA actuator configuration. COP values with work recovery therefore represent a theoretical upper bound for benchmarking future bidirectional actuator designs.".
- Added a clarifying note in *Supplementary Table 4* stating that: "COP values reported for the full system correspond to the one-way shape memory actuator configuration without work recovery. Values labeled "with work recovery" represent a theoretical upper bound of the cooling unit and are provided for benchmarking future bidirectional actuator designs."

Comment 8: *The scalability of the proposed system remains unclear. Applications shown in Supplementary Fig. 6 require cooling powers ranging from several watts to hundreds of watts, which are not addressed in the current design.*

Response: We thank the Reviewer for this important comment regarding scalability and absolute cooling power. We agree that the absolute cooling power (2.79 mW) is limited by the small active mass of the present thin-film prototype. The device was intentionally designed as a miniature proof-of-concept to validate thermally driven actuation, film-level integration, and coupled operation, rather than to maximize absolute cooling capacity.

To clarify scalability pathways, we have expanded the Discussion to outline physically realistic routes toward higher cooling power based on established film-based elastocaloric architectures:

- Parallelization of multiple films: Prior work (Ulpiani *et al.*, Ref. 19) has demonstrated proportional scaling of cooling capacity by integrating multiple SMA films in parallel, achieving a 4.5-fold increase when scaling from one to five films, reaching 0.9 W.
- Increasing lateral film dimensions: Because elastocaloric cooling power scales with actively cycled material volume under comparable stress and strain conditions, enlarging film width or active length increases total cooling capacity approximately proportionally, provided heat transfer remains sufficient.

- Modular integration: In thin-film architectures, multiple film stacks can share common heat sinks and heat sources, enabling power scaling without linear growth in system footprint.

We also clarify that scaling introduces engineering challenges, including synchronization of heat exchanger motion, uniform stress distribution across parallel films, and preservation of efficient heat transfer under higher thermal loads. These considerations are now explicitly discussed to provide a balanced and realistic scalability assessment.

We position the present work as establishing the feasibility of thermally driven thin-film elastocaloric integration, with scaling pathways analogous to previously demonstrated parallel film-based systems, rather than as a watt-scale commercial device.

Reference:

[19] Ulpiani, G. *et al.* Upscaling of SMA film-based elastocaloric cooling. *Applied Thermal Engineering* **180**, 115867 (2020).

Changes made:

- Expanded the *Discussion* to clarify scalability pathways as well as engineering constraints associated with scaling (Page 7, Line 276–287):

"The present prototype serves as a proof-of-concept platform for investigating scalability of film-based heat-driven elastocaloric cooling. Although the absolute cooling power is limited by the small active mass of the thin-film refrigerant, the total cooling capacity can be increased by (i) integrating multiple films in parallel and (ii) enlarging the lateral dimensions of each film, as demonstrated for film-based elastocaloric systems in Ref. 19. Because the cooling power scales approximately with the volume of actively cycled material under comparable stress and strain conditions, increasing the number or area of films can proportionally enhance total output. In the present architecture, modular integration with shared heat sinks and heat sources may mitigate footprint growth compared to duplicating complete device assemblies. However, scaling to higher cooling capacities will require careful control of actuator synchronization, uniform stress distribution across multiple films, and maintenance of efficient heat transfer at increased thermal loads.".

Reviewer 3's and 4's comments

This submission describes an interesting and elegant strategy to achieve cooling without minimal use of electricity. The authors used a thermally powered TiNi thin strip to induce the elastocaloric effect in a TiNiFe thin strip, coupled with controlled movement of a heat sink for the actuating strip and a pair of heat sink and source for the elastocaloric TiNiFe thin strip. Although the device presented does not appear to be a complete cooler system, the concept points to a new approach to harvesting waste or environmental heat for thermal management. The paper could be suitable for publication after the comments are addressed:

Response: We sincerely thank the Reviewers for their positive evaluation of our work and for recognizing the conceptual significance of thermally driven thin-film elastocaloric cooling. We appreciate the constructive feedback and thoughtful suggestions provided. We have carefully addressed all comments in detail below and revised the manuscript accordingly to improve clarity, rigor, and presentation.

Comment 1: *The actuator and refrigerant films form a push-pull couple. As the stroke of 300 um is much greater than the film thickness, buckling could occur when a film is pushed. Was buckling observed, and how was it overcome?*

Response: We thank the Reviewers for raising this important mechanical stability concern. Because the actuation stroke (~300 μm) significantly exceeds the film thickness, buckling is indeed a potential risk in push–pull operation.

In the present design, buckling was not observed during operation, as confirmed by Supplementary Videos 1 and 2. This stability is achieved primarily by applying an initial tensile pre-strain to both the actuator and refrigerant films. The pre-strain maintains tensile loading throughout cyclic operation and prevents compressive instability during push–pull motion.

In addition, compliant structural elements were incorporated to mitigate misalignment and ensure stable contact even in the event of slight out-of-plane deformation. Specifically: (1) A spring-like PLA cantilever supporting the actuation-unit heat sink reduces sensitivity to alignment errors and maintains controlled contact; (2) PDMS square rings work as buffers in the cooling-unit to provide compliant behavior to heat sink/source, minimizing alignment errors and sustains effective contact.

These measures collectively ensure buckling-free operation under the tested conditions. We have revised the manuscript to clarify these stabilization strategies.

Changes made:

- Added clarification in the *Methods* section (Page 7, Line 307–309, 317–320; Page 10, Line 422–424) describing the buckling-prevention strategies. The revised text reads:

"The pre-strain length was kept moderate, as larger pre-strains did not improve cooling performance. It also prevented buckling of both SMA films during push–pull operation."

"The spring-like compliant cantilever mitigates film–heat-exchanger misalignment and preserves stable thermal contact, even under minor buckling of the SMA films."

"PDMS square rings were placed around the PMMA support legs before assembly with the top and bottom PMMA plates to provide compliance. This design mitigates the effects of minor buckling in the refrigerant film and ensures stable, repeatable contact with the heat exchangers during operation."

Comment 2: *In the cooling device, the actuator is activated via Joule heating. It is recommended to use a direct heat source to activate the actuator? It is understandably that the heating using external heat would be slow, but it is important to demonstrate such truly thermally driven cooling. How about using hot and cold water to drive the actuator?*

Response: We thank the Reviewers for this important and technically insightful comment. We fully agree that demonstrating actuation driven by an external heat source is essential to validate the concept of truly thermally driven cooling.

To directly address this concern, we have implemented and experimentally validated a configuration in which Joule heating is completely replaced by an external heat source in the actuation unit. In this modified setup, thermal energy is supplied via solid–solid contact between the actuator film and a temperature-controlled copper plate heated by an external microheater. This eliminates internal Joule heating within the actuator and enables evaluation under boundary-driven heating conditions representative of practical low-grade thermal sources. Under identical film dimensions and operating frequency (0.83 Hz), the externally heat-driven system achieves:

- A device-level temperature span of 2.2 K
- A cooling power of 1.36 mW (temperature-slope method) and 2.09 mW (counter-heating method)
- A specific cooling power of 3.92 W g^{-1}

Although the performance is lower than that of the Joule-heated configuration (4.0 K span), this reduction is primarily attributed to thermally constrained strain rates and the shorter achievable stroke under the present actuator geometry. Importantly, the results confirm that elastocaloric cooling can be driven purely by externally supplied thermal energy under boundary-heating conditions, thereby validating the broader applicability of the heat-driven concept.

Regarding the suggestion of using hot and cold water as the driving source, such a fluid-based thermal actuation approach is conceptually feasible and may further improve heat-transfer rates. However, in the present miniature thin-film prototype, implementing fluidic actuation would introduce additional complexity and significantly alter the system architecture. The solid–solid contact configuration adopted here was chosen to isolate and validate the fundamental feasibility of boundary-driven thermal actuation.

We have added a dedicated section in the main text and Methods describing the externally heat-driven configuration, along with new figures and supplementary data detailing device architecture, actuation dynamics, and performance metrics. The distinction between Joule-heated and externally heat-driven operation is now clearly presented throughout the manuscript.

Changes made:

- Implemented and experimentally validated an externally heat-driven configuration using solid-to-solid thermal contact instead of internal Joule heating (new *Fig. 5* and related discussion).

- Added a new section "*Coupled heat-driven system using an external heat source*" (Page 6, Line 240–267) in the main text describing device design, operating parameters, and performance under external heat-source actuation.
- Added a new *Methods* subsection (Page 11, Line 464–485) detailing construction and operation of the externally heat-driven actuation unit.
- Added *Supplementary Figs. 6*, *9*, and *15* to document boundary-heating configuration, actuation dynamics, and working principle.
- Updated *Supplementary Fig. 7*, *Supplementary Tables 3* and *Supplementary Tables 4* to include cooling power, COP, and exergetic efficiency values for externally heat-driven operation.
- Revised *Abstract*, *Results*, and *Conclusion* to clearly distinguish between externally heat-driven configurations and Joule-heated.

For clarity, the **selected** key newly added figures and corresponding text passages are provided below:

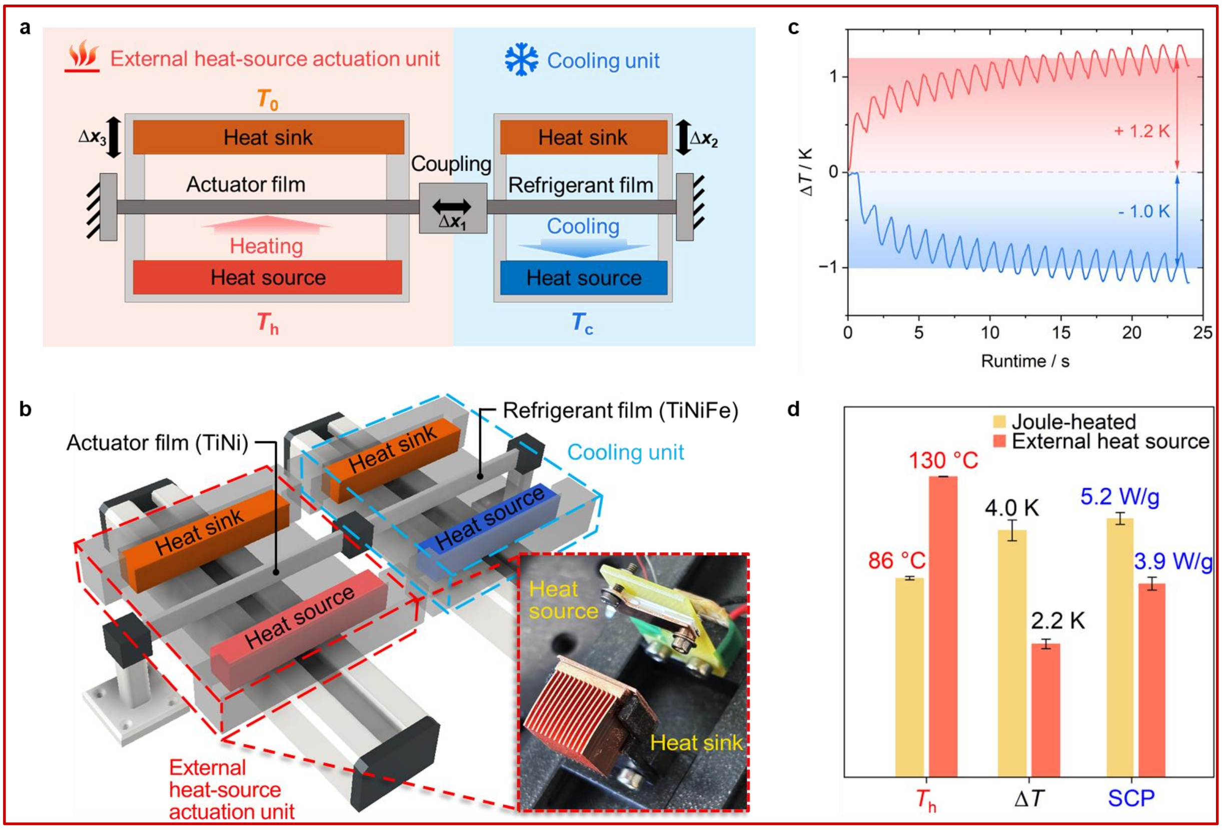

Fig. 5: System design and performance of the elastocaloric cooling device under external heat-source actuation. a, Schematic illustration of the device architecture, where Joule heating is replaced by an external solid heat source in the actuation unit, enabling thermal energy input through solid-to-solid contact. T_c, T_h, and T_0 denote the cooling temperature in the cooling unit, the heating temperature in the actuation unit, and the ambient temperature, respectively. **b**, Three-dimensional representation of the prototype showing the actuator film, refrigerant film, external heat source in the actuation unit, and the heat exchangers. Inset: close-up view of the fin-structured heat sink and the heat source assembly in the actuation unit. The heat source consists of a platinum microheater bonded to a thin Cu contact plate that interfaces with the actuator film. **c,** Device-level temperature span (ΔT) over 24 s of operation. After 20 cycles, a steady-state temperature span of 2.2 K is reached, corresponding to an average temperature rise of +1.2 K at the hot side and an average temperature drop of −1.0 K at the cold side. **d,** Comparison of heating temperature T_h, temperature span (ΔT), and specific cooling power (SCP, counter-heating method) between Joule-heated actuation and external heat-source actuation. The proof-of-concept external heat-source configuration exhibits lower performance

primarily due to the reduced actuation stroke under the current geometric constraints. Data are shown as mean ± standard deviation (n = 3 independent experiments).

New section "*Coupled heat-driven system using an external heat source*" in the Main text (Page 6, Line 240–267):

"To verify true heat-driven operation, Joule heating was replaced with an external solid heat source in the actuation unit, enabling direct conductive heating of the actuator film (Fig. 5a, b). The verification prototype was operated using the same film dimensions and cycling frequency as the Joule-heated configuration to allow direct comparison. The external heat source was maintained at 130 °C (T_h) to provide sufficient thermal input for uniaxial loading of the refrigerant film by approximately 300 μm within a 0.25 s heating interval (Supplementary Fig. 9a). Active motion control of the heat source and heat sink in the actuation unit constrained the loading and unloading durations to approximately 0.6 s (Supplementary Fig. 9b, c), corresponding to strain rates between 0.053 s^{-1} to 0.066 s^{-1} (Supplementary Fig. 9d).

Cooling performance was evaluated under these conditions, with the heating time increased to 0.35 s to ensure sufficient thermal input in the coupled heat-driven system using an external heat source. With a slightly reduced stroke (strain ≈ 4.1%), the externally heat-driven device achieves a steady-state temperature span of 2.2 K at the same operating frequency as the Joule-heated coupled system (Fig. 5c, d). The cooling power at zero temperature lift, determined using the counter-heating method, is 2.09 mW, corresponding to a specific cooling power of 3.92 W g^{-1} (Supplementary Fig. 7 and Supplementary Table 3). When the heat sink in the cooling unit is maintained near ambient temperature, the cold-side temperature drop ($T_c - T_0$) increases from −1.0 K to −1.4 K (Supplementary Fig. 6b).

Compared to the Joule-heated configuration, the externally heat-driven system exhibits reductions of 1.8 K in temperature span and 1.32 W g^{-1} in specific cooling power (Fig. 5d), primarily due to the lower achievable stroke under the present actuator geometry. The higher required heating temperature of 130 °C, compared to 86 °C in the Joule-heated case, reflects the different heat-transfer mechanisms involved. Joule heating generates volumetric internal heat, whereas the external heat source relies on boundary-driven conduction. Optimization of actuator geometry and transformation temperature A_f, together with improved heat-transfer design, may reduce the required heat source temperature and enhance actuation efficiency in future implementations.".

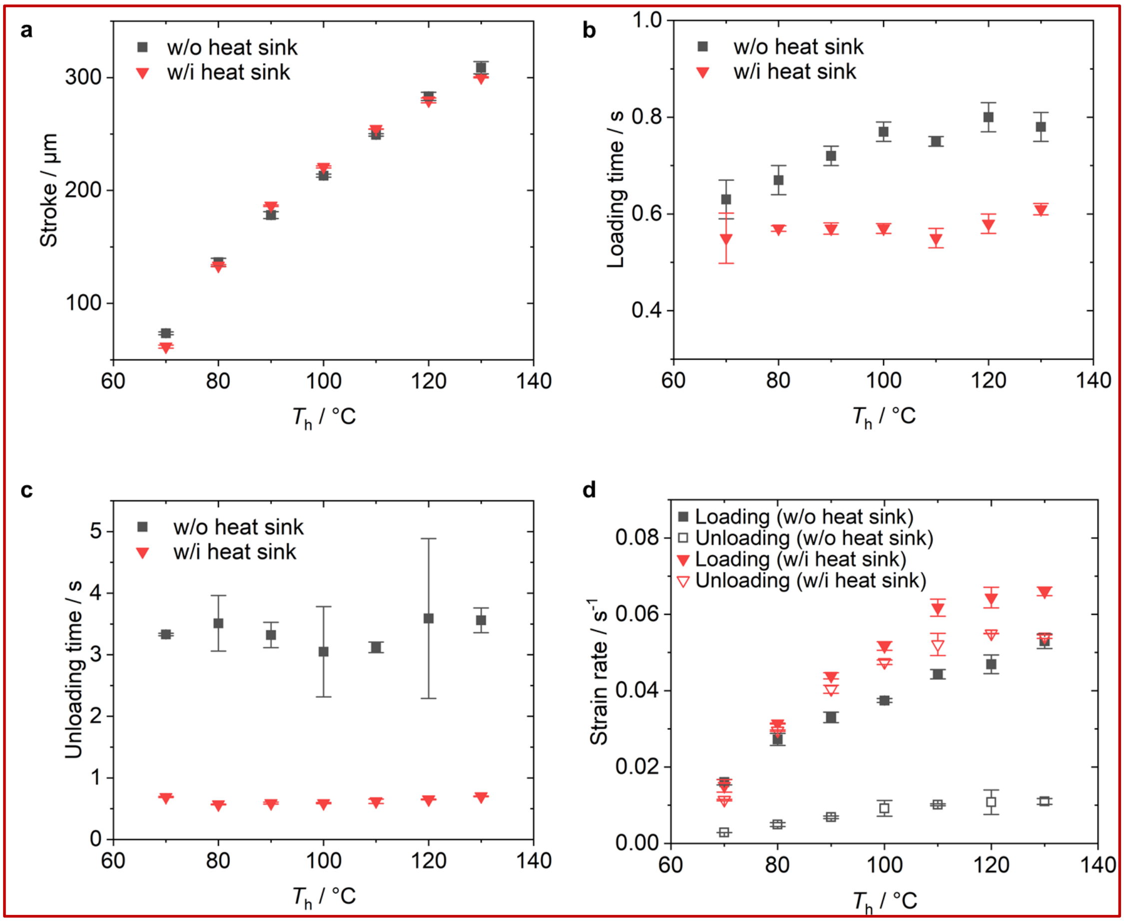

Supplementary Fig. 9. Performance of the external heat-source actuation unit at heat-source temperatures from 70 to 130 °C with a 250 ms contact time. Data obtained without and with implementation of the heat sink are shown in black and red, respectively. **a,** Actuation stroke as a function of heat-source temperature (T_h). At 130 °C, strokes exceed 300 µm for both configurations, providing sufficient strain to load the refrigerant film. **b,** Loading time versus T_h. Without active heat-sink implementation, loading times range from approximately 0.6 to 0.8 s. Incorporating active heat-sink movement reduces the loading time to 0.6 s and improves consistency. **c,** Unloading time versus T_h. Without active heat-sink control, unloading exceeds 3 s and shows significant variability due to uncontrolled convective cooling of the actuator film. With active heat-sink implementation, unloading time is constrained to 0.6 s, markedly improving repeatability. **d,** Corresponding strain rates during loading and unloading. Active heat-sink control increases both loading and unloading strain rates, approaching the adiabatic regime, reaching 0.07 s^{-1} (loading) and 0.05 s^{-1} (unloading) at 130 °C. Data are shown as mean ± standard deviation (n = 3 independent experiments).

Supplementary Table 3. Cooling power of Joule-heated and externally heat-driven elastocaloric systems determined by temperature-slope calculation and direct counter-heating measurement.

Actuation mode	$T_0 - T_c$ (K)	Cooling power (temperature-slope) (mW)	Cooling power (counter-heating) (mW)
Joule-heated actuation	0	3.08	2.79
	1	–	1.25
	2	–	0

External heat-source actuation	0	1.36	2.09
	0.5	–	1.27
	1	–	0

Cooling power determined using the temperature-slope method is derived from the initial temperature decay rate of the heat source under zero temperature lift conditions. Accordingly, values from the temperature-slope method are only provided for $T_0 - T_c = 0$ K. Cooling power determined using the counter-heating method is obtained as described in the Methods section. "–" indicates not applicable.

New section in the *Methods* (Page 11, Line 464–485):

"The external heat source was fabricated in-house using a 5 × 5 mm^2 platinum microheater (Innovative Sensor Technology). The microheater was bonded with thermally conductive adhesive to a 0.6 mm-thick Cu plate, which served as the contact interface with the actuator film. A thermocouple was attached to the Cu plate for closed-loop PID temperature control. A fin-structured Cu heat sink was employed to remove heat from the actuator film during the cooling stage.

The heat-source temperature was varied between 70 and 130 °C with a 250 ms contact time to determine the required heating temperature, T_h, for achieving sufficient loading stroke and acceptable loading/unloading times (Supplementary Fig. 9). The device operates in a four-step cycle, as illustrated in Supplementary Fig. 15. The operating frequency was set to 0.83 Hz, identical to that of the Joule-heated configuration for direct comparison. The loading and unloading velocities were 507 µm/s (stain rate 0.07 s^{-1}) and 511 µm/s (stain rate 0.07 s^{-1}), respectively.

Cooling power was determined using both the temperature-slope method and the direct counter-heating method. At zero temperature lift, the cooling powers obtained from the temperature-slope method and the counter-heating method are 1.36 mW and 2.09 mW, respectively (Supplementary Fig. 7 and Supplementary Table 3). The slightly higher value obtained from the counter-heating method may reflect increased sensitivity to ambient disturbances at low power levels, whereas the temperature-slope method may underestimate cooling power due to unaccounted thermal mass in surrounding components. COP values at zero temperature lift and exergetic efficiency at a −0.5 K temperature drop, evaluated under different input-power definitions, are summarized in Supplementary Table 4.

Comment 3: *It is unclear how rapid heat transfer between the SMA films and the heat sinks and source was obtained. Provide relevant experimental details with illustration or images to facilitate the description.*

Response: We thank the Reviewers for highlighting the need for clearer documentation of the heat-transfer dynamics between the SMA films and the heat exchangers.

To address this comment, we experimentally analyzed the transient thermal response of the refrigerant film in contact with the heat sink and heat source at 0.83 Hz operation. The temperature evolution of the heat exchangers during the 500 ms contact period is now provided in Supplementary Fig. 16. From these measurements, thermal equilibrium is reached within approximately 270 ms for the heat sink and 350 ms for the heat source. Both values are significantly shorter than the available contact duration, confirming that sufficient heat exchange occurs within each cycle.

To further substantiate this, we performed a lumped-capacitance analysis of the thermal time constant. The experimentally derived time constant (τ ≈ 62 ms) agrees well with theoretical estimation based on an effective interfacial conductance of approximately 1150 W m^{-2} K^{-1}. The calculated Biot numbers (Bi ≪0.1) validate the lumped-system assumption. These results demonstrate that interfacial heat transfer is sufficiently rapid under the applied contact pressure.

The detailed calculation, parameter definitions, and validation are now provided in *Supplementary Note 2*, and the heat-transfer pathway and transient temperature profiles are illustrated in *Supplementary Fig. 16*.

Changes made:

- Added *Supplementary Fig. 16* illustrating the heat-transfer pathway and transient temperature evolution of the heat sink and heat source.
- Added a new paragraph in the *Methods* section (Page 10, Line 426–430) quantifying experimentally measured heat-transfer times and reporting the derived thermal time constant.
- Added *Supplementary Note 2* providing detailed lumped-capacitance analysis, Biot number validation, and calculation of effective interfacial conductance.

For clarity, the **key** newly added figures and corresponding text passages are provided below:

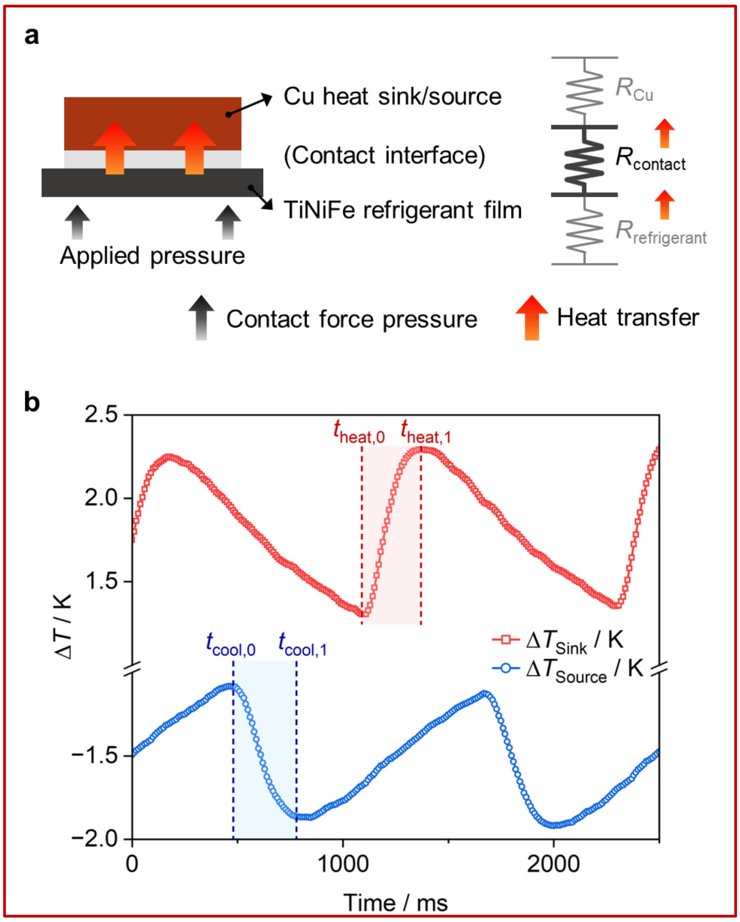

Supplementary Fig. 16. Heat-transfer time between refrigerant film and heat sink/source in the cooling unit. a, Schematic illustration of the heat-transfer pathway from the refrigerant film through the contact interface to the Cu heat sink/source when mechanical pressure is applied. The internal thermal resistances of the refrigerant film ($R_{refrigerant}$) and Cu heat exchanger (R_{Cu}) are assumed negligible due to their small thicknesses and high thermal conductivities, such that the interfacial resistance ($R_{contact}$) dominates the heat-transfer process. **b,** Temperature evolution of the heat sink and heat source during contact with the refrigerant film at 0.83 Hz operation and 500 ms contact duration. The heat sink approaches thermal equilibrium within approximately 270 ms ($t_{heat,0}$ to $t_{heat,1}$), while the heat source requires approximately 350 ms ($t_{cool,0}$ to $t_{cool,1}$). Both values are shorter than the total contact time, indicating sufficient time for effective heat exchange during each cycle. Symbols represent experimental data; lines are guides to the eye.

A new paragraph in the *Methods* section (Page 10, Line 426–430): "The average heat transfer times between the refrigerant film and the heat sink and heat source were approximately 270 ms and 350 ms, respectively, as determined from the temperature evolution of the heat exchangers. The experimentally derived thermal time constant ($\tau \approx 62$ ms) agrees well with theoretical estimation (see Supplementary Note 2 for details)."

Supplementary Note 2. Detailed calculation of thermal time constant for heat transfer between refrigerant film and heat sink/source.

The heat-transfer pathway is schematically illustrated in Supplementary Fig. 16a. During operation, heat flows from the refrigerant film through the solid–solid contact interface to the copper heat sink or heat source when mechanical pressure is applied.

The overall thermal resistance consists of three components: the internal resistance of the refrigerant film ($R_{refrigerant}$), the interfacial contact resistance ($R_{contact}$), and the internal resistance of the Cu heat exchanger (R_{Cu}). Due to the small thickness and relatively high thermal conductivity of both the refrigerant film and the Cu heat exchanger, their internal thermal resistances are negligible compared to the interfacial resistance. Therefore, the lumped-capacitance approximation is applicable.

The validity of lumped system analysis is assessed using the Biot number:

$$Bi = \frac{h_{\text{contact}} L_c}{k}$$

where $h_{contact}$ is the interfacial thermal conductance, k is thermal conductivity, and L_c is the characteristic length. When $Bi << 0.1$, spatial temperature gradients within the solid are negligible.

Under this assumption, the thermal time constant τ of the refrigerant film is given by:

$$\tau = \frac{\rho_{\text{refrigerant}}\, L_{\text{c,refrigerant}}\, c_{\text{p,refrigerant}}}{h_{\text{contact}}}$$

where $\rho_{refrigerant}$ is density, $c_{p,refrigerant}$ is specific heat capacity, and $L_{c,refrigerant}$ is the characteristic length.

Typical interfacial conductance values for solid–solid contact under moderate pressure range from 1000 to 3000 W/m^2 K. Using these values yields a theoretical thermal time constant in the range of 23–71 ms.

The temperature evolution of the heat sink and heat source in the Joule-heated configuration (0.83 Hz frequency, 500 ms contact time) is shown in Supplementary Fig. 16b. The heat sink approaches thermal equilibrium after approximately 270 ms ($t_{heat,0}$ to $t_{heat,1}$), while the heat source requires approximately 350 ms ($t_{cool,0}$ to $t_{cool,1}$). Effective heat transfer therefore occurs within the available 500 ms contact duration.

A first-order thermal system reaches more than 99% equilibrium after approximately 5τ. Based on the experimentally observed equilibrium time of ~310 ms, the corresponding time constant is:

$$\tau \approx 62 \text{ ms}$$

Using this experimentally derived time constant, the effective interfacial conductance is calculated as:

$$h_{\text{contact}} \approx 1150 \text{ W/m}^2 \text{ K}$$

This value falls within the expected range for solid–solid interfaces under moderate pressure, confirming consistency between theoretical estimation and experimental observation.

The parameters used in the above calculations are summarized below.

Parameter	Definition	Value	Unit
$L_{\mathrm{c,refrigerant}}$	Characteristic length of refrigerant film	26×10^{-6} **	m
$L_{\mathrm{c,Cu}}$	Characteristic length of Cu heat sink/source	600×10^{-6} **	m
$k_{\mathrm{refrigerant}}$	Thermal conductivity of refrigerant film	18 *	W/m K
k_{Cu}	Thermal conductivity of Cu heat sink/source	400 *	W/m K
h_{contact}	Interfacial conductance	1150	W/m^2 K
$Bi_{\mathrm{refrigerant}}$	Biot number of refrigerant film	0.0014	–
Bi_{Cu}	Biot number of Cu heat sink/source	0.0017	–
$\rho_{\mathrm{refrigerant}}$	Density of refrigerant film	6460 ***	Kg/m^3
$c_{\mathrm{p,refrigerant}}$	Specific heat capacity of refrigerant film	500	J/kg K

* Values obtained from literature (see Ref. 2)

** Experimental measured values

*** Calculated from nominal atomic composition using atomic weights from Ref. 2.

Comment 4: *Provide information of the operating stability of the device? How many cycles can this device run without an obvious deterioration in its cooling performance?*

Response: We thank the Reviewers for raising the important question of operating stability.

To evaluate short-term cyclic stability, the Joule-heated heat-driven elastocaloric device was operated continuously for 80 cycles (96 s at 0.83 Hz). Throughout this test, the device-level temperature span (~4.0 K) and the maximum loading force remained stable, indicating consistent thermomechanical performance.

A moderate reduction in stroke was observed during the initial cycles, followed by gradual stabilization. Importantly, the minimum stroke remained above 330 µm, exceeding the design threshold of 300 µm required to fully transform the refrigerant film. As a result, no deterioration in cooling performance was observed during the 80-cycle test.

It is important to note that the present first-generation prototype was primarily designed to demonstrate the feasibility of heat-driven elastocaloric cooling rather than to optimize long-term fatigue lifetime. Accordingly, fatigue-optimized SMA compositions and structural lifetime engineering were not implemented in this device. Under these proof-of-concept conditions, the actuator film fractured after the 82nd cycle, and performance beyond this cycle count is therefore not reported. Importantly, this limitation reflects the current prototype configuration rather than an intrinsic fatigue constraint of thin-film SMA materials. Ultra-low-fatigue TiNi-based thin films reported in the literature, such as Ti-rich TiNiCu and TiNiCuCo alloys, have demonstrated stable cyclic performance exceeding 10^7 cycles under tensile actuation without functional degradation[42–44]. These alloy systems are compatible with thin-film elastocaloric architectures. Combined with structural optimization to reduce stress concentration and thermal accumulation, they provide a clear pathway toward substantially extending operational lifetime in future device iterations.

Supplementary Fig. 14 has been added to document temperature span, force–stroke behavior, and cycle-resolved stroke and force evolution.

Reference:

[42] Chluba, C. *et al*. Ultralow-fatigue shape memory alloy films. *Science* **348**, 1004–1007 (2015).
[43] Chluba, C., Ossmer, H., Zamponi, C., Kohl, M. & Quandt, E. Ultra-Low Fatigue Quaternary TiNi-Based Films for Elastocaloric Cooling. *Shap. Mem. Superelasticity* **2**, 95–103 (2016).
[44] Ossmer, H., Chluba, C., Kauffmann-Weiss, S., Quandt, E. & Kohl, M. TiNi-based films for elastocaloric microcooling— Fatigue life and device performance. *APL Mater.* **4**, 064102 (2016).

Changes made:

- Added *Supplementary Fig. 14* summarizing (i) temperature span stability, (ii) force–stroke hysteresis at selected cycles, and (iii) cycle-resolved stroke and maximum force.

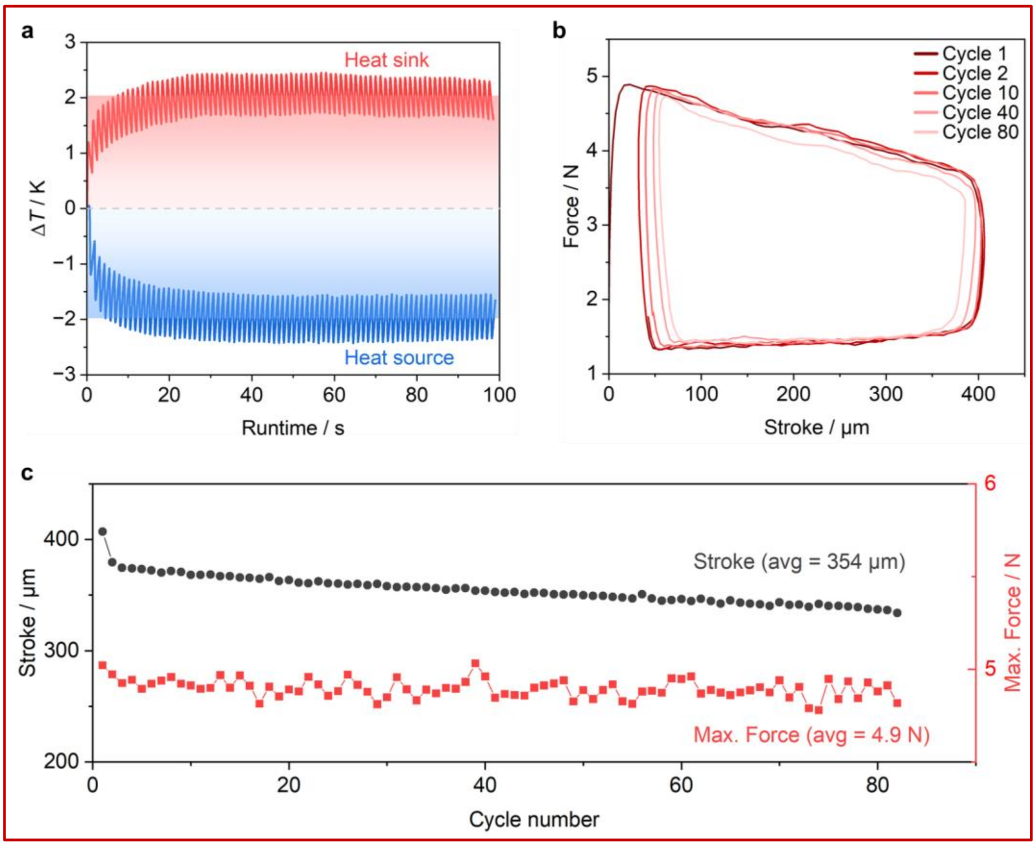

Supplementary Fig. 14. Stability of the Joule-heated heat-driven elastocaloric cooling system over 80 cycles. a, Device-level temperature span (ΔT) during 80 consecutive cycles (96 s) at 0.83 Hz, showing a stable steady-state span of approximately 4.0 K. **b,** Force–stroke hysteresis loops of the coupled actuator–refrigerant system at selected cycles (1, 2, 10, 40, and 80), demonstrating reproducible mechanical response during cyclic operation. **c,** Cycle-resolved actuation stroke and maximum force. The stroke exhibits an initial decrease after the first cycle followed by gradual stabilization, with an average value of 354 μm and a minimum value above 330 μm, remaining above the design threshold of 300 μm throughout the test. The maximum force remains stable with an average of 4.9 N, indicating sustained mechanical loading capability of the refrigerant film. Symbols represent experimental data; lines are guides to the eye.

- Added a new paragraph in the *Methods* section (Page 10, Line 430–433) describing the 80-cycle stability test under Joule-heated actuation and reporting temperature span, stroke, and force evolution:

"A stability test performed under Joule-heated actuation for 80 cycles (96 s) showed no degradation in temperature span or maximum loading force. Although a slight reduction in stroke was observed, the minimum value remained above the designed threshold of 300 μm, resulting in stable cooling performance (Supplementary Fig. 14)."

- Clarified in the manuscript that the reported stability reflects a first-generation proof-of-concept prototype and that lifetime optimization will be addressed in future developments (Page 8, Line 351–363):

"The fatigue behavior of the superelastic TiNiFe refrigerant film was evaluated under tensile loading at 5.2% strain and a strain rate of 0.02 s^{-1}. The film sustained more than 2000 cycles without mechanical failure or observable functional degradation, confirming mechanical robustness within the operating strain range of the present prototype. However, the primary objective of this work was to establish a proof-of-concept demonstration of heat-driven elastocaloric cooling rather than to optimize long-term cyclic lifetime. Consequently, fatigue-optimized SMA compositions were not specifically implemented in the current device. Notably, ultra-low-fatigue TiNi-based thin films have been reported in the literature. Ti-rich TiNiCu and TiNiCuCo films have demonstrated stable cyclic performance exceeding 10^7 cycles under tensile actuation without functional degradation[42–44]. These alloy systems are fully compatible with thin-film elastocaloric architectures. Combined with improved mechanical design to minimize stress concentration and thermal accumulation, they provide a clear pathway toward substantially extending operational lifetime in future device generations."

Comment 5: *What is the total length and width of the TiNiFe film in the cooling unit?*

Response: We thank the Reviewers for pointing out the need for clearer dimensional information of the TiNiFe refrigerant film.

The TiNiFe refrigerant film has a total length of 13.0 mm and consists of a central rectangular gauge section with ring-shaped ends for clamping, as illustrated in the inset of Fig. 2a. Each ring has an inner diameter of 1.0 mm and an outer diameter of 2.5 mm to ensure precise alignment during clamping. The active rectangular gauge section between the two rings is 7.5 mm long and 0.5 mm wide.

For clarity and completeness, these dimensions have now been explicitly added to the *Methods* section.

Changes made:

- Added a new paragraph in the *Methods* section (Page 8, Line 339–342) specifying the geometry and dimensions of the TiNiFe refrigerant film: "The refrigerant film consists of a 13.0 mm-long strip with ring-shaped ends, as shown in the inset of Fig. 2a. Each ring has an inner diameter of 1.0 mm and an outer diameter of 2.5 mm, providing precise alignment during clamping. The rectangular gauge section between the two rings is 7.5 mm long and 0.5 mm wide."

Comment 6: *What is the speed of the stretching that the actuator film can generate when it is coupled to the refrigerant film? Can faster stretching speed of the actuator film result in a larger adiabatic temperature change in the refrigerant film and thus better performance at the device level?*

Response: We thank the Reviewers for this insightful question regarding actuation speed and its influence on cooling performance.

In the coupled configuration, the actuator film generates loading and unloading velocities of approximately 639 μm s^{-1} (0.09 s^{-1} strain rate) and 526 μm s^{-1} (0.07 s^{-1} strain rate), respectively, when driving the refrigerant film under Joule-heated operation. For the externally heat-driven configuration, the loading and unloading velocities are 507 μm s^{-1} and 511 μm s^{-1} (both ~0.07 s^{-1} strain rate).

Regarding the second question, higher stretching speeds would indeed increase the strain rate and bring the refrigerant film closer to adiabatic conditions. For the present TiNiFe film, fully adiabatic temperature change (~19.4 K) is achieved under high strain-rate tensile testing. In the coupled device, however, the attainable strain rates remain slightly below the commonly accepted adiabatic threshold (~0.1 s^{-1}), resulting in partial heat exchange with the surroundings during transformation and thus a reduced material-level temperature span (12.9 K) and device-level span (4.0 K).

Nevertheless, increasing stretching speed alone is not sufficient to guarantee improved device-level performance. Higher strain rates must be accompanied by enhanced heat-transfer rates and careful frequency optimization to prevent thermal accumulation and parasitic heat leakage. Therefore, device-level cooling performance is governed by a coupled balance between actuation dynamics, heat-transfer efficiency, and cycle timing.

To clarify these points, we have revised the manuscript to explicitly report loading/unloading velocities and to discuss future pathways for increasing strain rate through actuator geometry optimization and alternative actuation strategies.

Changes made:

- Added explicit loading and unloading velocities (μm s^{-1}) for both Joule-heated and externally heat-driven configurations in the *Methods* section:

  a. For coupled heat-driven system (Joule-heated actuation) (Page 10, Line 441–443): "Fully adiabatic conditions typically require strain rates ≥ 0.1 s^{-1} (≈ 750 μm/s), whereas the present actuator provides 0.09 s^{-1} during loading (≈ 639 μm/s) and 0.07 s^{-1} during unloading (≈ 526 μm/s)."

  b. For coupled heat-driven system (external heat-source actuation) (Page 11, Line 475–476): "The loading and unloading velocities were 507 μm/s (stain rate 0.07 s^{-1}) and 511 μm/s (stain rate 0.07 s^{-1}), respectively."

- Added clarification in the *Methods* section regarding how strain rate influences the adiabatic temperature change (Page 11, Line 439–444): "In both cases, the limitation originates from thermally constrained actuation dynamics, which restrict both the strain rate and the achievable operating frequency…These sub-adiabatic strain rates allow partial heat exchange during phase transformation."

- Added a discussion paragraph in the *Methods* section addressing potential strategies for increasing strain rate and improving device-level performance (Page 10, Line 448–453): "Future improvements may focus on increasing strain rates through optimized actuator geometry, enhanced heat transfer, or alternative actuation strategies to more fully exploit the intrinsic cooling potential of the refrigerant film. Advanced actuation concepts, including bistable configurations, agonist–antagonist designs, or catch-and-release mechanisms[46,47], together with multistage cascading architectures on the cooling side[15,45], may further enhance the effective device-level temperature span."

Reference:

[46] Chen, X., Bumke, L., Quandt, E. & Kohl, M. Bistable Actuation Based on Antagonistic Buckling SMA Beams. *Actuators* 12, 422 (2023).
[47] Bevilacqua, D. *et al.* Performance analysis of agonist-antagonist SMA micro-wires and resonant compliant joint in bio-inspired bat-like flapping wings. in *Bioinspiration, Biomimetics, and Bioreplication XIV* vol. 12944 33–42 (SPIE, 2024).

Comment 7: *A miniaturized thermocouple is attached to the backside of the Cu heat sink to measure the temperature. What is the size of this thermocouple and how do you ensure that the temperature profile along the Cu heat sink is uniform and the reading of thermocouple can reflect the actual temperature of the Cu strip?*

Response: We thank the Reviewers for raising this important point regarding temperature measurement accuracy.

Device-level temperatures were measured using miniature type-K thermocouples with a tip diameter of 360 µm and sensing wire diameter of 80 µm. The small dimensions were intentionally selected to minimize additional thermal mass and reduce measurement disturbance.

To verify spatial temperature uniformity of the Cu heat source, we performed a comparative measurement using two thermocouples: one positioned at the center (TC_{mid}) and another located 0.5 mm from the edge (TC_{side}). The temperature difference between TC_{mid} and TC_{side} remained below 0.1 K under all tested operating conditions (Supplementary Fig. 13b). Given the high thermal conductivity of Cu and the small lateral dimensions of the heat source, this small deviation confirms a nearly homogeneous temperature distribution along the strip. Therefore, the temperature measured at TC_{mid} is representative of the overall heat-source temperature during device operation.

Changes made:

- Added thermocouple dimensions (tip diameter: 360 µm; sensing wire diameter: 80 µm) in the *Methods* section (Page 9, Line 391).
- Added a description of dual-position temperature validation (TC_{mid} and TC_{side}) in the *Methods* section.
- Included quantitative validation (<0.1 K difference) supporting the homogeneous temperature assumption (Page 9, Line 392–396): "To verify that TC_{mid} accurately represents the overall heat-source temperature, an additional thermocouple (TC_{side}) was placed near the edge of the heat source. The temperature difference between TC_{mid} and TC_{side} remained below 0.1 K throughout operation (Supplementary Fig. 13b), confirming a spatially homogeneous temperature distribution across the heat source during cycling.".
- Added *Supplementary Fig. 13* illustrating thermocouple geometry, placement, and measured temperature differences.

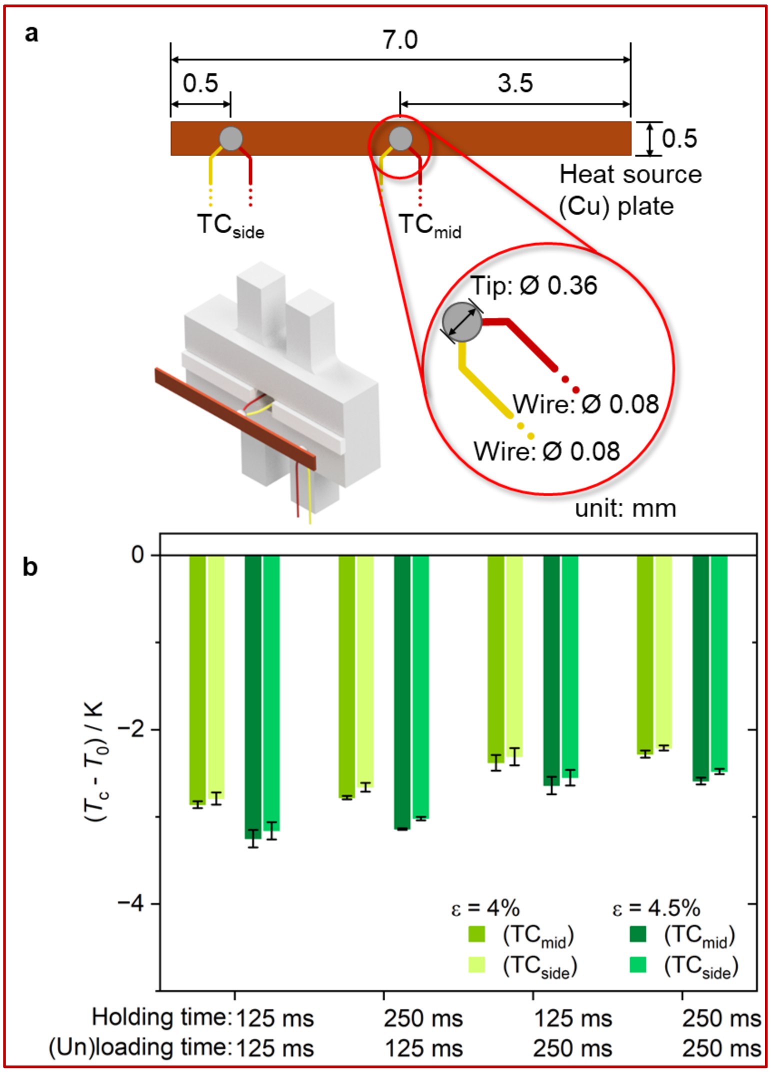

Supplementary Fig. 13. Validation of thermocouple measurement positions at the heat source in the cooling unit. a, Schematic illustration of the heat-source geometry (dimensions in mm) and thermocouple measurement locations. All device-level temperatures reported in the cooling unit are measured at the center of the heat source (TC_{mid}). An additional thermocouple (TC_{side}) was positioned near the edge of the heat source to verify spatial temperature uniformity. **b,** Comparison of temperature differences ($T_c - T_0$) measured at TC_{mid} and TC_{side} under 4% and 4.5% strain conditions using electromechanical actuation. The temperature difference between the two measurement positions remains below 0.1 K for all tested conditions, confirming a homogeneous temperature distribution across the heat source and validating the use of TC_{mid} as a representative measurement point. Detailed numerical values are provided in Supplementary Table 1. Data are presented as mean ± standard deviation (n = 3 independent experiments).

Comment 8: *Can you show the detailed calculation of the cooling power (the specific numbers you plugged in Q = msourcecp, sourceTsource)?*

Response: We thank the Reviewers for requesting clarification of the cooling-power calculation. To improve transparency, we now explicitly list all constant numerical parameters used in the cooling-power evaluation in Supplementary Table 2, including the heat-source mass, heat capacity, and active refrigerant mass.

Cooling power determined by the temperature-slope method is calculated as:

$$\dot{Q}_{\mathrm{c}} = m_{\mathrm{source}} c_{\mathrm{p,source}} \dot{T}_{\mathrm{source}}$$

where m_{source}= 3.14 mg is the mass of the Cu heat source, $c_{p,\mathrm{source}}$= 0.385 J/g °C, and $\dot{T}_{\mathrm{source}}$ is the experimentally extracted initial cooling rate of the heat source during the first cycle at zero temperature lift. Because $\dot{T}_{\mathrm{source}}$ is obtained directly from the measured temperature–time curve and varies between experiments, it is not tabulated as a fixed parameter.

The specific cooling power is obtained as:

$$\dot{q}_{\mathrm{c}} = \frac{\dot{Q}_{\mathrm{c}}}{m_{\mathrm{SE}}}$$

where m_{SE} = 0.533 mg is the active mass of the refrigerant film. All constant numerical inputs used in the calculation are provided in Supplementary Table 2.

In addition, cooling power was independently determined using a direct counter-heating method, in which a calibrated 0.5 Ω NiCr resistance wire supplies electrical power to the heat source until thermal balance is reached. The electrical power required to offset the cooling effect is taken as the cooling power. The close agreement between the two methods supports the validity of the evaluation.

Changes made:

- Revised the *Methods* section (Page 11, Line 491–508) to explicitly describe cooling-power evaluation using both the temperature-slope method and the independent counter-heating method.
- Added *Supplementary Table 2* listing all constant parameters used in the cooling-power calculation.

Supplementary Table 2. Parameters used for cooling power and specific cooling power calculations.

Parameter	Definition	Value	Unit
ρ_{source}	Density of Cu heat source	8.96 *	g/cm^3
V_{source}	Volume of Cu heat source	0.35 **	mm^3
m_{source}	Mass of Cu heat source	3.14	mg
$c_{\mathrm{p,source}}$	Specific heat capacity of Cu	0.385 *	J/g °C
ρ_{SE}	Density of refrigerant film ($Ti_{49.1}Ni_{50.5}Fe_{0.4}$)	6.46 ***	g/cm^3
V_{SE}	Volume of refrigerant film (active region)	0.083 **	mm^3
m_{SE}	Mass of refrigerant film (active region)	0.533	mg

Footnotes

* Values obtained from literature (see Ref. 2)

** Experimentally measured values.

*** Calculated from nominal atomic composition using atomic weights from Ref. 2.

Reference:

[1] Rumble, J. R. *CRC Handbook of Chemistry and Physics: A Ready-Reference Book of Chemical and Physical Data*. (CRC Press, Taylor & Francis Group, 2021).

Comment 9: *Is it possible for you to use a heat flux sensor to measure the cooling power? This measurement would be more direct.*

Response: We thank the Reviewers for suggesting the use of a heat-flux sensor for direct cooling-power measurement. In the present miniaturized thin-film prototype, commercially available heat-flux sensors are significantly larger than the active heat-exchange area and would introduce substantial additional thermal mass and contact resistance, thereby perturbing the thermal dynamics of the system and compromising measurement accuracy.

Instead, following the Reviewer's suggestion for a more direct evaluation, we implemented an independent counter-heating method. In this approach, a calibrated 0.5 Ω NiCr resistance wire supplies electrical power to the heat source until thermal equilibrium is reached. The electrical power required to offset the cooling effect is taken as the cooling power. This method provides a direct energy-balance measurement at the heat source and is well suited to the milliwatt-scale cooling powers of the present device.

We now provide a systematic comparison between cooling powers obtained from the temperature-slope method and the counter-heating method in Supplementary Fig. 7 and Supplementary Table 3. The close agreement between the two methods supports the reliability of the cooling-power evaluation.

The manuscript has been revised accordingly to clearly distinguish between the two determination methods and to report both values consistently.

Changes made:

- Revised the *Methods* section (Page 11, Line 491–508) to explicitly describe cooling-power determination using both the temperature-slope method and the independent counter-heating method.
- Added *Supplementary Fig. 7* comparing cooling powers obtained from both methods.
- Added *Supplementary Table 3* summarizing cooling powers determined by the temperature-slope method and the direct counter-heating method under different operating conditions.

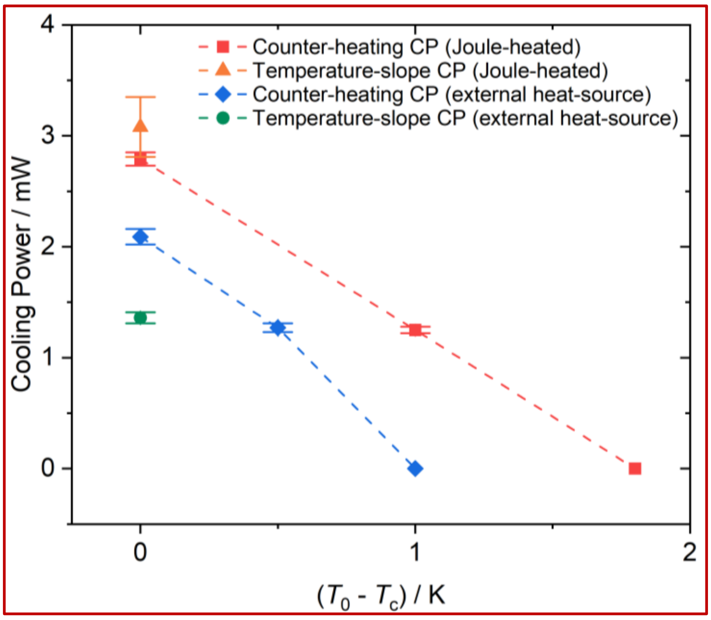

Supplementary Fig. 7. Cooling power under different actuation modes and determination methods. Cooling power values for the Joule-heated actuation configuration are shown in red (counter-heating method) and orange (temperature-slope method). Cooling power values for the external heat-source actuation configuration are shown in blue (counter-heating method) and green (temperature-slope method). Cooling power determined using the temperature-slope method is derived from the initial temperature decay rate of the heat source during the first cooling cycle at zero temperature lift. Cooling power determined using the counter-heating method is obtained by supplying electrical power through a calibrated resistance wire to offset the cooling effect. The parameters used in the temperature-slope analysis are listed in Supplementary Table 2, and detailed numerical values of cooling power are provided in Supplementary Table 3. Data are presented as mean ± standard deviation (n = 3 independent experiments). Symbols represent experimental data points, and dashed lines serve as guides to the eye.

Supplementary Table 3. Cooling power of Joule-heated and externally heat-driven elastocaloric systems determined by temperature-slope calculation and direct counter-heating measurement.

Actuation mode	$T_0 - T_c$ (K)	Cooling power (temperature-slope) (mW)	Cooling power (counter-heating) (mW)
Joule-heated actuation	0	3.08	2.79
	1	–	1.25
	2	–	0
External heat-source actuation	0	1.36	2.09
	0.5	–	1.27
	1	–	0

Cooling power determined using the temperature-slope method is derived from the initial temperature decay rate of the heat source under zero temperature lift conditions. Accordingly, values from the temperature-slope method are only provided for $T_0 - T_c$ = 0 K. Cooling power determined using the counter-heating method is obtained as described in the Methods section. "–" indicates not applicable.

Comment 9: *What causes the large discrepancy between the material temperature span and the device temperature span?*

Response: We thank the Reviewers for raising this important point. The discrepancy between material-level and device-level temperature span arises from thermodynamic and heat-transfer limitations inherent to dynamic device operation.

At the material level, the maximum adiabatic temperature change (ΔT_{ad} = 19.4 K) is measured under high strain-rate tensile testing, where heat exchange with the surroundings is negligible. Under device operation, however, the effective temperature change is reduced primarily due to sub-adiabatic strain rates. The present actuator operates at 0.09 s^{-1} during loading and 0.07 s^{-1} during unloading, slightly below the ≥0.1 s^{-1} typically required for fully adiabatic conditions. Consequently, partial heat exchange occurs during phase transformation, yielding a material-level temperature change of 12.9K rather than the fully adiabatic value.

At the device level, the temperature span is further limited by finite heat-transfer rates between the refrigerant film and the heat exchangers, as well as by the thermal mass of the heat sink and heat source during cyclic operation. In addition, the present system employs a single-stage architecture without regeneration or cascading[15, 45], which is known to yield device-level spans significantly lower than intrinsic material ΔT_{ad}. As a result, while the material exhibits a quasi-adiabatic temperature change of 12.9 K, the coupled device achieves a 4.0 K temperature span under continuous operation, and 8.2 K in the cooling-only configuration.

We have revised the manuscript to explicitly clarify these mechanisms.

Changes made:

- Added a paragraph in the *Methods* section (Page 10, Line 434–453) explaining strain-rate limitations, finite heat-transfer effects, and architectural constraints that reduce device-level temperature span.
- Included quantitative strain-rate values and comparison to adiabatic conditions.
- Added references (15, 45–47) to contextualize the expected reduction in device-level performance in non-regenerative systems.

"The material-level temperature change of 12.9 K for TiNiFe films under Joule-heated thermal actuation is lower than the fully adiabatic value of 19.4 K measured under high strain-rate tensile testing. This reduction arises from the limited strain rate during device operation. Likewise, the device-level temperature span of 4.0 K in the coupled heat-driven configuration remains below the maximum 8.2 K achieved in the cooling-only unit driven by an electromechanical actuator. In both cases, the limitation originates from thermally constrained actuation dynamics, which restrict both the strain rate and the achievable operating frequency. Fully adiabatic conditions typically require strain rates ≥ 0.1 s^{-1} (≈ 750 µm/s), whereas the present actuator provides 0.09 s^{-1} during loading (≈ 639 µm/s) and 0.07 s^{-1} during unloading (≈ 526 µm/s). These sub-adiabatic strain rates allow partial heat exchange during phase transformation. At the device level, the temperature span is further limited by finite heat-transfer rates between the refrigerant film and the heat sink/source, as well as the thermal mass of the heat exchangers during cyclic operation. In the absence of regenerative or cascaded architecture[15,45], the net temperature lift accumulated per cycle remains lower than the intrinsic material temperature change. Future improvements may focus on increasing strain rates through optimized actuator geometry, enhanced heat transfer, or alternative actuation strategies to more fully exploit the intrinsic cooling potential of the refrigerant film. Advanced actuation concepts, including bistable configurations, agonist–antagonist designs, or catch-and-release mechanisms[46,47], together with multistage cascading architectures on the cooling side[15,45], may further enhance the effective device-level temperature span."

Reference:

[15] Xu, J. *et al.* SMA Film-Based Elastocaloric Cooling Devices. *Shap. Mem. Superelasticity* **10**, 119–133 (2024).

[45] Snodgrass, R. & Erickson, D. A multistage elastocaloric refrigerator and heat pump with 28 K temperature span. *Sci Rep* **9**, 18532 (2019).

[46] Chen, X., Bumke, L., Quandt, E. & Kohl, M. Bistable Actuation Based on Antagonistic Buckling SMA Beams. *Actuators* **12**, 422 (2023).

[47] Bevilacqua, D. *et al.* Performance analysis of agonist-antagonist SMA micro-wires and resonant compliant joint in bio-inspired bat-like flapping wings. in *Bioinspiration, Biomimetics, and Bioreplication XIV* vol. 12944 33–42 (SPIE, 2024).

Comment 10: *If you use a Cu heat sink with a larger heat mass (for example, a thicker Cu strip) but the heat source stays unchanged, could a larger temperature span or more cooling be obtained in the heat source?*

Response: We thank the Reviewers for this insightful question regarding the effect of heat-sink thermal mass on device performance.

In the initial experiments, the heat sink was insulated to evaluate the maximum achievable total temperature span (ΔT_{total}) of the cooling unit. However, in practical applications the heat sink would be maintained near ambient temperature. Following the Reviewers' suggestion, we conducted additional experiments using a heat sink with larger thermal mass to maintain its temperature within ~1 K of ambient.

For the stand-alone cooling unit driven by an electromechanical actuator, maintaining the heat sink near ambient reduced the total temperature span by approximately 2.0 K, due to suppression of hot-side temperature rise. Importantly, however, the cold-side temperature drop ($T_c - T_0$) increased by an average of 0.8 K, indicating enhanced effective cooling performance under application-relevant boundary conditions (Supplementary Fig. 4 and Supplementary Table 1).

We further performed analogous tests for the coupled systems. In the Joule-heated configuration, the cold-side temperature drop remained at −1.8 K when switching from an insulated heat sink to a heat sink maintained near ambient temperature (Supplementary Fig. 6a), suggesting that performance is presently limited by actuation frequency and heat-transfer dynamics rather than hot-side thermal accumulation. In contrast, in the externally heat-driven configuration, maintaining the heat sink near ambient increased the cold-side temperature drop from −1.0 K to −1.4 K (Supplementary Fig. 6b).

These results demonstrate that increasing heat-sink thermal mass does not increase total temperature span, but can enhance cold-side cooling when the hot side is stabilized near ambient temperature. The manuscript has been revised to clarify this behavior.

Changes made:

- Added a paragraph in the *Discussion* (Page 5, Line 183−191) describing the effect of heat-sink boundary conditions on temperature span and cold-side drop in the cooling-only unit.
- Added discussion of heat-sink stabilization effects in both the Joule-heated and externally heat-driven coupled configurations (Page 5, Line 209−212; Page 6, Line 256−258).
- Added *Supplementary Fig. 4* and *Supplementary Fig. 6* comparing insulated and ambient-controlled heat-sink conditions.
- Added *Supplementary Table 1* summarizing detailed temperature-span data under different heat-sink boundary conditions.

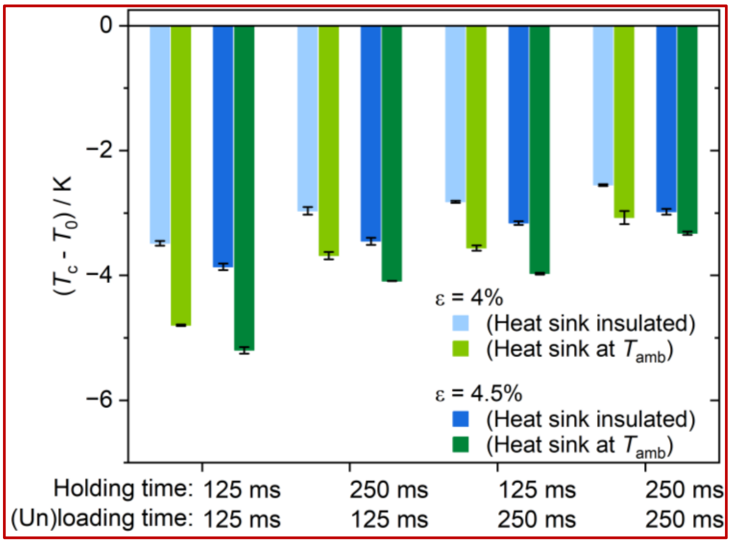

Supplementary Fig. 4. Comparison of temperature drop ($T_c - T_0$) under different heat-sink boundary conditions and strain ε. Temperature drops were measured using the stand-alone cooling unit driven by electromechanical actuators. Results are shown for ε = 4% and ε = 4.5% at different (un)loading and holding times (125 ms and 250 ms). Light blue and dark blue bars represent ε = 4% and ε = 4.5%, respectively, with the heat sink insulated. Light green and dark green bars represent ε = 4% and ε = 4.5%, respectively, with the heat sink maintained at ambient temperature (T_{amb}). Maintaining the heat sink near ambient temperature using a larger thermal mass (limiting the hot-side temperature rise to <1 K above ambient) increases the temperature drop by an average of 0.8 K compared to the insulated condition. Detailed numerical values are provided in Supplementary Table 1. Data are shown as mean ± standard deviation (n = 3 independent experiments).

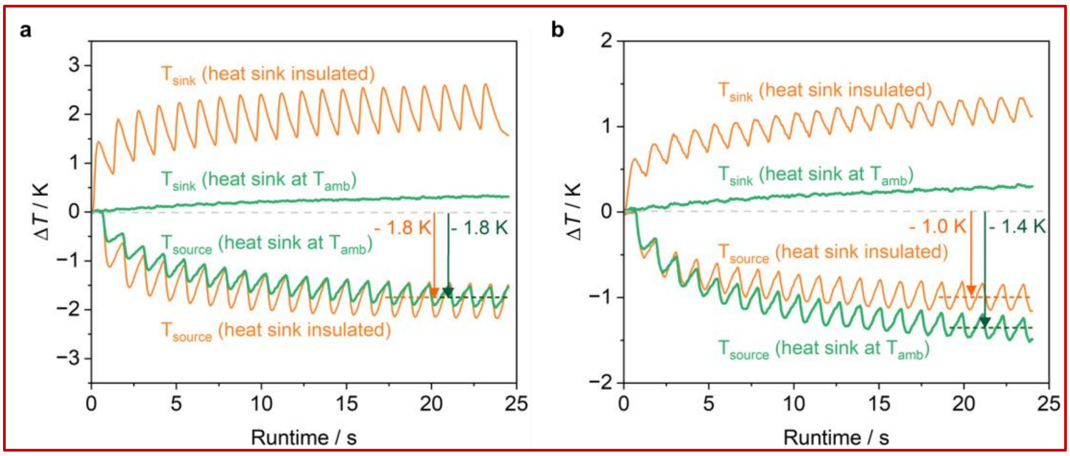

Supplementary Fig. 6. Effect of heat-sink boundary conditions on temperature drop ($T_c - T_0$) for (a) Joule-heated and (b) externally heat-driven elastocaloric devices. a, In the Joule-heated actuation configuration, the temperature drop remains unchanged at −1.8 K whether the heat sink is insulated or maintained near ambient temperature. **b,** In the externally heat-driven configuration, maintaining the heat sink near ambient temperature increases the temperature drop from −1.0 K (insulated) to −1.4 K. In both panels, orange curves correspond to the insulated heat-sink condition, and green curves correspond to the heat sink maintained near ambient temperature.

Supplementary Table 1. Device-level total temperature span ($\Delta T_{total} = T_h - T_c$) and cold-side temperature drop ($\Delta T_c = T_c - T_0$) of the stand-alone elastocaloric cooling unit driven by electromechanical actuators under different boundary conditions, applied strain, and timing parameters. Holding/(un)loading time refers to the duration of thermal contact and mechanical loading/unloading, respectively.

Conditions					
Heat sink	Heat source	Strain ε	Holding/ (Un)loading time (ms)	ΔT_{total} (K)	ΔT_c (K)
Insulated	Insulated	4.0 %	125 / 125	7.2	− 3.5
			250 / 125	6.0	− 3.0
			125 / 250	5.7	− 2.8
			250 / 250	5.1	− 2.6
		4.5 %	125 / 125	8.2	− 3.9
			250 / 125	7.2	− 3.5
			125 / 250	6.6	− 3.2
			250 / 250	6.1	− 3.0
Maintained at T_{amb}	Insulated	4.0 %	125 / 125	5.5	− 4.8
			250 / 125	4.2	− 3.7
			125 / 250	4.1	− 3.6
			250 / 250	3.5	− 3.1
		4.5 %	125 / 125	5.9	− 5.2
			250 / 125	4.7	− 4.1
			125 / 250	4.5	− 4.0
			250 / 250	3.8	− 3.3
Maintained at T_{amb}	Measured with two thermocouples (TC_{mid} position)	4.0 %	125 / 125	–	− 2.9
			250 / 125	–	− 2.8
			125 / 250	–	− 2.4
			250 / 250	–	− 2.3
		4.5 %	125 / 125	–	− 3.3
			250 / 125	–	− 3.1
			125 / 250	–	− 2.6
			250 / 250	–	− 2.6
	Measured with two thermocouples (TC_{side} position)	4.0 %	125 / 125	–	− 2.8
			250 / 125	–	− 2.7
			125 / 250	–	− 2.3
			250 / 250	–	− 2.2
		4.5 %	125 / 125	–	− 3.2
			250 / 125	–	− 3.0
			125 / 250	–	− 2.6
			250 / 250	–	− 2.5

Response Letter

We sincerely thank the Editor and the Reviewers for their careful evaluation of our manuscript entitled: "*Heat-driven Elastocaloric Cooling using Shape Memory Films*" and for the opportunity to further revise it. We greatly appreciate the constructive comments, which have helped us improve the clarity, rigor, and positioning of the manuscript.

We have carefully addressed all points raised by the reviewers. Reviewer comments are reproduced in **blue**. Our responses are provided in **black**. Revisions made in the manuscript are shown in **red**.

Below we respond to each comment in detail.

Editor's comments

Comment 1: *Reviewer #2 has raised points that need to be addressed before we can make a decision on publication.*

Response: We have carefully addressed all comments raised by Reviewer #2 and revised the manuscript accordingly. Detailed responses are provided below.

Reviewer 1’s comments

The authors significantly improved their manuscript with a clear point-to-point reply to the reviewer's comment. Therefore, it can be recommended for publication.

Response: We sincerely thank the Reviewer for the positive evaluation of our work and for recognizing the improvements made in the revised manuscript. We greatly appreciate the constructive feedback provided during the review process, which has helped us strengthen the clarity and quality of the manuscript.

Reviewer 2's comments

The authors have substantially expanded the manuscript by adding new experimental data, supplementary materials, and demonstrations of heat driven cooling using an external heat source. They have also provided detailed responses to the concerns raised by all three referees. These additions improve the clarity and completeness of the work, and the revised version reads significantly better than the original submission.

However, several of the newly added materials still contain technical inconsistencies or incomplete explanations. The authors must address the following issues before the manuscript can meet the publication standards of Nature Energy.

Response: We sincerely thank the Reviewer for the careful evaluation of our manuscript and for the constructive and detailed feedback. We appreciate the recognition of the improvements made in the revised version. We have carefully addressed all points raised and revised the manuscript accordingly. Detailed responses to each comment are provided below.

Comment 1: *The authors should include video documentation of the prototype operating with the external heat source to maintain consistency with the Joule heated demonstration.*

Response: We thank the Reviewer for this suggestion regarding consistency of experimental demonstration. Following this recommendation, we have added *Supplementary Video 4* showing the operation of the external heat-source-driven actuation unit. Since the cooling unit remains unchanged between the Joule-heated and externally heat-driven configurations, the existing video of the cooling unit (Supplementary Video 1) is applicable to both cases. Together, these videos provide a complete demonstration of the system under both actuation modes.

Changes made:

- Added *Supplementary Video 4* showing the operation of the external heat-source-driven actuation unit.
- Updated the Discussion section (Page 6, Line 262-263) to reference the new video:

"The operation of the external heat-source-driven actuation unit is shown in Supplementary Video 4.".

Comment 2: *The expanded discussion of COP and exergetic efficiency is valuable, but key information is still missing. Specifically, the transient development of the temperature span under different external loads shown in Supplementary Fig. 7 should be added, and the temperatures used to calculate exergetic efficiency should be included in Supplementary Table 4.*

Response: We thank the Reviewer for this valuable comment. To address this point, we have added the transient evolution of temperature under different external thermal loads in Supplementary Fig. 7b. These measurements correspond to the operating points (i)–(vi) shown in Supplementary Fig. 7a and provide direct insight into the dynamic behavior underlying the cooling power evaluation. In the counter-heating method, the heat source is preheated using a resistance wire to establish a controlled thermal load, after which the elastocaloric system is activated while the electrical heating is maintained throughout the measurement to reach steady-state conditions.

In addition, we have now explicitly included the corresponding temperature values (T_0, T_c, and T_h) used for the exergetic efficiency calculations in Supplementary Table 4. This ensures full transparency of all thermodynamic inputs under different operating conditions.

Changes made:

- Added *Supplementary Fig. 7b* showing the transient evolution of temperature under different external thermal loads, corresponding to points (i)–(vi) in Supplementary Fig. 7a.

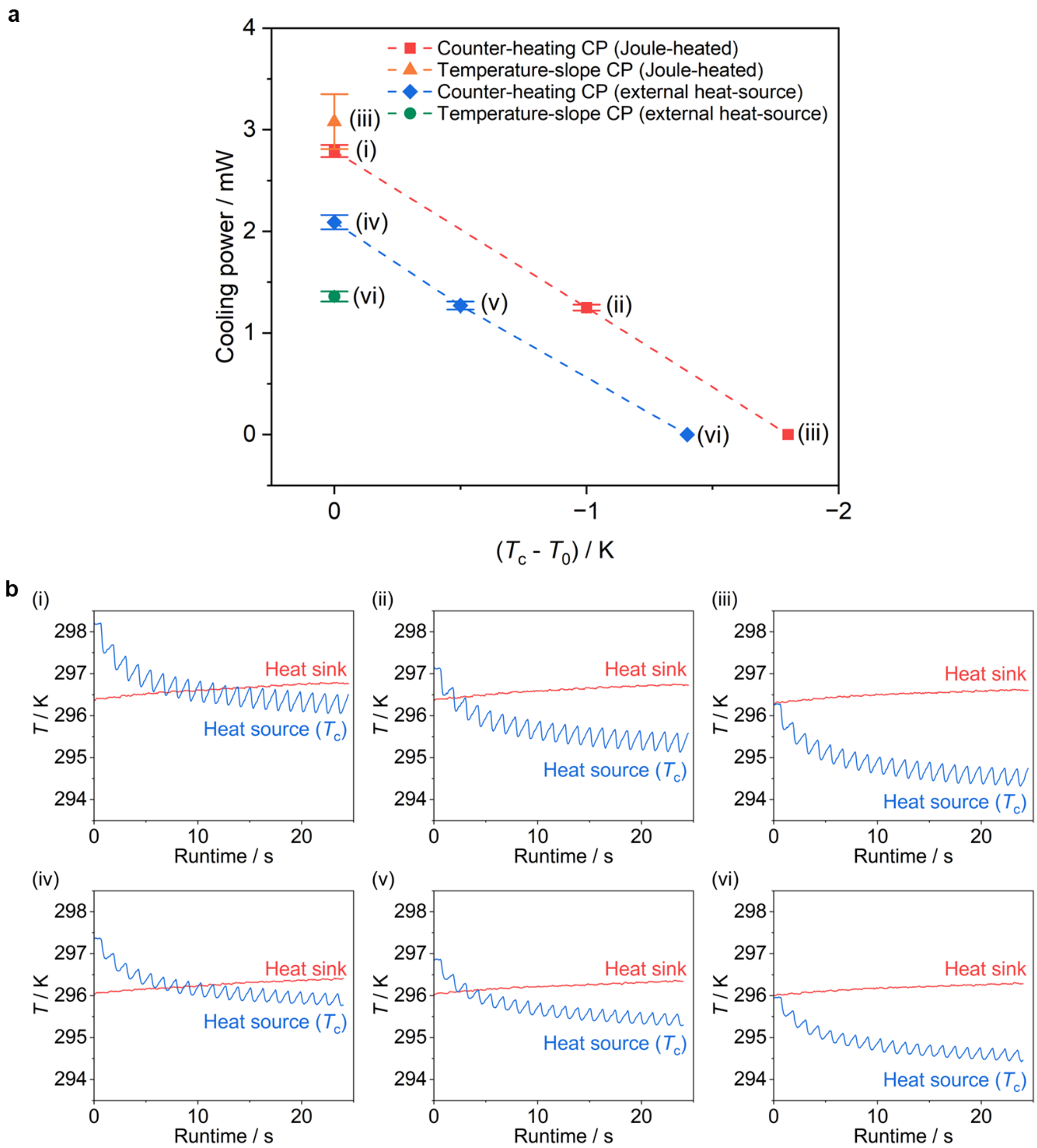

Supplementary Fig. 7. Cooling power under different actuation modes and determination methods. a, … Labels (i)−(vi) correspond to the transient temperature evolution under different external thermal loads shown in panel **b**. Data are presented as mean ± standard deviation (n = 3 independent experiments). Symbols represent experimental data points, and dashed lines serve as guides to the eye. **b,** Transient evolution of temperature under different external thermal loads. Red curves represent the temperature of the heat sink which remains close to ambient temperature, while blue curves represent the temperature of the heat source (T_c). In the counter-heating measurements, the heat source is preheated using a resistance wire to establish a controlled thermal load, after which the elastocaloric system is activated while the electrical heating is maintained to reach steady-state conditions.

- Revised the *Methods* section (Page 12 Line 514–518) to describe the counter-heating measurement procedure and the applied thermal loading conditions.

"In the counter-heating method, a calibrated 0.5 Ω NiCr resistance wire is used to electrically supply heat to the heat source until thermal balance is reached, and the electrical input power required to offset the cooling effect is taken as the cooling power. To establish controlled thermal loading conditions, the heat source is preheated using the resistance wire for 60 s prior to actuation. Subsequently, the elastocaloric system is activated to induce cooling, while the electrical heating is maintained throughout the measurement. The resulting temperature evolution under different thermal loads is shown in Supplementary Fig. 7b."

- Updated *Supplementary Note 2* to explicitly reference *Supplementary Table 4* for temperature inputs used in exergetic efficiency calculations.

"The corresponding values of T_0, T_c, and T_h under different operating conditions are provided in Supplementary Table 4."

- Expanded *Supplementary Table 4* to include T_0, T_c, and T_h under all evaluation conditions, and clarified their definitions in the table caption.

Supplementary Table 4. Coefficient of performance (COP) and exergetic efficiency of Joule-heated and externally heat-driven elastocaloric systems under different evaluation criteria. Definitions of COP and exergetic efficiency, including the corresponding input-power bases, are provided in Supplementary Note 2. T_0 denotes the ambient temperature, T_c the heat-source temperature in the cooling unit, and T_h the actuator temperature (Joule-heated case) or the external heat-source temperature.

Evaluation conditions		COP	Exergetic efficiency
Joule heating actuation		evaluated at $T_c - T_0 = 0$ K	evaluated at $T_c - T_0 = -1$ K (T_c = 294.3 K) (T_0 = 295.3 K) (T_h = 359.7 K)
Temperature-slope method	Cooler (with work recovery)	5.46	–
	Cooler (without work recovery)	2.88	–
	Thermal actuator efficiency (thermal input basis)	~~0.03~~ 3.27×10^{-2}	–
	Thermal actuator efficiency (electrical input basis)	~~0.01~~ 8.37×10^{-3}	–
	Full system (thermal input basis)	~~0.09~~ 9.43×10^{-2}	–
	Full system (electrical input basis)	~~0.02~~ 2.41×10^{-2}	–

	Full system (thermal input basis + auxiliary actuators)	~~0.0008~~ 7.56×10^{-4}	–
	Full system (electrical input basis + auxiliary actuators)	~~0.0007~~ 7.39×10^{-4}	–
Counter-heating method	Cooler (with work recovery)	4.94	4.21 %
	Cooler (without work recovery)	2.61	2.22 %
	Thermal actuator efficiency (thermal input basis)	~~0.03~~ 3.27×10^{-2}	3.27 %
	Thermal actuator efficiency (electrical input basis)	~~0.01~~ 8.37×10^{-3}	~~0.84 %~~ 0.837 %
	Full system (thermal input basis)	~~0.09~~ 8.53×10^{-2}	~~0.07 %~~ 7.27×10^{-2} %
	Full system (electrical input basis)	~~0.02~~ 2.18×10^{-2}	~~0.02 %~~ 1.86×10^{-2} %
	Full system (thermal input basis + auxiliary actuators)	~~0.0007~~ 6.85×10^{-4}	~~0.001 %~~ 5.84×10^{-4} %
	Full system (electrical input basis+ auxiliary actuators)	~~0.0007~~ 6.69×10^{-4}	~~0.001 %~~ 5.71×10^{-4} %
External heat-source actuation		evaluated at $T_c - T_0 = 0$ K	evaluated at $T_c - T_0 = -0.5$ K (T_c = 295.1 K) (T_0 = 295.6 K) (T_h = 403.2 K)
Temperature-slope method	Cooler (with work recovery)	2.31	–
	Cooler (without work recovery)	1.50	–
	Thermal actuator efficiency (electrical input basis)	~~0.0024~~ 2.43×10^{-3}	–
	Full system (electrical input basis)	~~0.0036~~ 3.63×10^{-3}	–
	Full system (electrical input basis+ auxiliary actuators)	~~0.0002~~ 2.05×10^{-4}	–
Counter-heating method	Cooler (with work recovery)	3.55	1.37 %
	Cooler without work recovery	2.31	~~0.89 %~~ 0.892 %

Thermal actuator efficiency (electrical input basis)	~~0.0024~~ 2.43×10^{-3}	~~0.24 %~~ 0.243 %
Full system (electrical input basis)	~~0.0056~~ 5.60×10^{-3}	~~0.002 %~~ 2.16×10^{-3} %
Full system (electrical input basis+ auxiliary actuators)	~~0.0003~~ 3.17×10^{-4}	~~< 0.001 %~~ 1.22×10^{-4} %

Comment 3: *In Supplementary Fig. 7, the noticeable discrepancy between the green dot and the blue diamond at 0 K requires further clarification to ensure the accuracy of the presented trends.*

Response: We thank the Reviewer for highlighting this point. The observed discrepancy at ΔT ≈ 0 K arises from the different evaluation principles of the two methods. In the counter-heating method, the cooling power is inferred from the electrical power required to maintain thermal balance. Parasitic heat exchange with the ambient environment constitutes a larger fraction of the applied heating power, which can lead to a slight overestimation of the cooling power[49]. In contrast, the temperature-slope method relies on the initial cooling rate of the heat source, which can be influenced by finite thermal response times associated with contact resistance and the thermal mass of surrounding components, resulting in a slight underestimation of the cooling power[18]. As a result, the two methods exhibit opposite systematic tendencies, leading to a difference between the evaluated values. We have revised the manuscript to clarify this behavior.

Changes made:

- Expanded the *Methods* section (Page 11 Line 491−500) to clarify the origin of the difference between the temperature-slope and counter-heating methods, including their respective systematic tendencies.

"The small difference between the two methods arises from their distinct evaluation principles. In the counter-heating method the cooling power is inferred from the electrical power required to maintain thermal balance. Parasitic heat exchange with the ambient environment contributes to the applied heating power, which can lead to a slight overestimation of the cooling power[48]. In contrast, the temperature-slope method relies on the initial cooling rate of the heat source, which can be influenced by finite thermal response times associated with contact resistance and the thermal mass of surrounding components, resulting in a slight underestimation of the cooling power[18]. As a result, the two methods exhibit opposite systematic tendencies, leading to a difference between the evaluated values."

Reference:

18. Bruederlin, F., Ossmer, H., Wendler, F., Miyazaki, S. & Kohl, M. SMA foil-based elastocaloric cooling: from material behavior to device engineering. *J. Phys. D: Appl. Phys.* **50**, 424003 (2017).

48. Ziolkowski, P., Blaschkewitz, P. & Müller, E. Heat flow measurement as a key to standardization of thermoelectric generator module metrology: A comparison of reference and absolute techniques. *Measurement* **167**, 108273 (2021).

Comment 4: *The caption of Supplementary Fig. 9 refers to operation "without active heat sink implementation" and to "significant variability due to uncontrolled convective cooling," but it is* *unclear whether this means the SMA dissipates heat directly to ambient air without contacting a heat sink, and this ambiguity should be resolved. Moreover, the claim that the results "highlight the potential of low grade thermal energy" is not supported given that the revised experiments require a substantially higher driving temperature of 130 °C compared to 86 °C in the Joule heated case.*

Response: We thank the Reviewer for this important comment. We have revised the caption of Supplementary Fig. 9 to clarify that, in the absence of an active heat sink, the actuator film dissipates heat directly to the ambient air through convection without solid–solid thermal contact.

Regarding the statement that the results "highlight the potential of low-grade thermal energy," we agree that this wording could be misleading. Based on the Reviewer's comment, we have revised the manuscript by removing references to low-grade thermal energy.

Changes made:

- Revised the caption of *Supplementary Fig. 9* to clarify that "without active heat sink" refers to heat dissipation of the actuator film directly to ambient air without solid–solid thermal contact:

"**Supplementary Fig. 9. … c,** Unloading time versus T_h. In the absence of an active heat sink, the actuator film dissipates heat directly to the ambient air without solid–solid thermal contact. Under these conditions, unloading times exceeds 3 s and exhibit significant variability due to uncontrolled convective cooling. …".

- Revised the *Abstract* (Page 1, Line 18; Line 24), *Discussion* (Page 7, Line 279−280), and *Conclusion* (Page 7, Line 301; Line 311) to remove references to low-grade thermal energy:

"This approach is expected to harness abundant ~~low-temperature~~ heat sources, such as waste heat or solar thermal energy..."

"These results mark a step toward sustainable, electricity-minimized elastocaloric cooling technologies that transform ~~low-grade~~ heat into useful cold."

"Similarly, in automotive systems, the device can be configured to manage thermal loads in on-board electronics, with the actuator films potentially powered by ~~low-grade~~ waste heat sources such as exhaust or drivetrain heat, …"

"We present an integrated film-based heat-driven elastocaloric cooler that converts ~~low-grade~~ thermal energy into mechanical work to drive solid-state refrigerants."

"These results demonstrate the feasibility of film-based heat-driven elastocaloric cooling and highlight the potential of ~~low-grade~~ thermal energy as a driving source for electricity-minimized thermal management systems."

Comment 5: *The response regarding scalability remains insufficient, as citing two approaches from prior work does not address the core issue that distributing external heat uniformly across multiple SMA elements in a parallel configuration introduces additional thermal resistance that is not accounted for in the current proof of concept system.*

Response: We thank the Reviewer for highlighting the important issue of scalability. We agree that distributing external heat across multiple elements introduces additional thermal resistance and represents a key challenge for system-level upscaling. The present work is intended as a proof-of-concept demonstration and therefore does not yet incorporate optimized heat-delivery architectures for scaled systems.

Scaling to higher cooling capacities requires careful management of heat delivery, as larger systems involve increased thermal loads. This necessitates optimized heat-distribution pathways to ensure uniform temperature fields and efficient operation. Potential mitigation strategies include the use of high-conductivity intermediate thermal layers to homogenize temperature distribution, enhanced heat-transfer interfaces to reduce thermal resistance, and modular architectures that minimize heat transport distances by locally coupling heat sources and active elements. In addition, actuator synchronization and uniform stress distribution across multiple films must be addressed.

We have revised the manuscript to explicitly acknowledge these challenges and to clarify that scalability has not yet been experimentally validated and requires further investigation in future work.

Changes made:

- Revised the *Discussion* section (Page 7 Line 290−299) to explicitly acknowledge the challenges associated with heat distribution and thermal resistance in scaled systems, and to clarify that upscaling is not addressed in the present work and requires further investigation in future development:

"However, scaling to higher cooling capacities requires careful management of heat delivery, as larger systems involve increased thermal loads. This necessitates optimized heat-distribution pathways to ensure uniform temperature fields and efficient operation. Potential mitigation strategies include the use of high-conductivity intermediate thermal layers to homogenize temperature distribution, enhanced heat-transfer interfaces to reduce thermal resistance, or modular architectures that minimize heat transport distances by locally coupling heat sources and active elements. In addition, actuator synchronization and uniform stress distribution across multiple films must be addressed. These aspects are not yet implemented in the current prototype and will require further investigation and engineering development in future work."

Comment 6: *The trends in Supplementary Fig. 4 and Fig. 6 are inconsistent, since Tc is always lower when the heat sink is at Tamb in Fig. 4, whereas the opposite trend appears in Fig. 6, and this contradiction must be resolved.*

Response: We thank the Reviewer for this careful observation. We agree that the apparent inconsistency between Supplementary Fig. 4 and Supplementary Fig. 6a requires clarification.

The two figures correspond to different system configurations with distinct performance limitations. In Supplementary Fig. 4, the temperature drop was measured using the stand-alone cooling unit driven by an electromechanical actuator, which enables higher actuation frequency (1−2 Hz) and strain rate (0.16−0.36 s^{-1}), allowing the system to operate closer to its intrinsic cooling performance. Under these conditions, maintaining the heat sink near ambient temperature effectively enhances heat rejection, resulting in a larger temperature drop at the heat source. In contrast, Supplementary Fig. 6a corresponds to the Joule-heated, thermally actuated coupled system, where the performance is limited by the actuation dynamics rather than the heat sink condition. Due to the lower operating frequency (0.83 Hz) and reduced strain rate (loading: 0.09 s^{-1}; unloading: 0.07 s^{-1}) imposed by thermal actuation, the achievable cooling capacity is constrained, and parasitic heat dissipation during non-contact intervals becomes more significant. As a result, the influence of heat sink conditions on the temperature drop is diminished, leading to the observed difference in trends.

We have revised the manuscript to clarify the distinction between these two operating regimes and to explain the origin of the differing trends.

Changes made:

- Revised the *Discussion* section (Page 5 Line 211−214) to clarify the origin of the temperature-drop behavior in the Joule-heated configuration and to explain the differing trends compared to the cooling-only system:

"The temperature drop (T_c – T_0) remains at −1.8 K when switching from an insulated heat sink to a heat sink maintained near ambient temperature (Supplementary Fig. 6a), indicating that under the current operating frequency, additional enhancement of the cold-side temperature drop is not observed. This differs from the cooling-only configuration (Supplementary Fig. 4), where higher electromechanical actuation frequency makes the heat sink condition a dominant factor. In contrast, in the Joule-heated coupled system, the lower operating frequency and strain rate limit the cooling capacity, reducing the influence of the heat sink condition."

Comment 7: *Supplementary Note 1 introduces the force displacement ratio, but the manuscript does not specify the ideal target value or how closely the demonstrated system approaches it, and this metric requires clearer explanation.*

Response: We thank the Reviewer for this insightful comment. We have revised Supplementary Note 1 to explicitly define the target force–displacement ratio based on the mechanical loading requirements of the refrigerant film. Specifically, a transformation force of 5–6 N and a corresponding displacement of 300–375 µm (4–5% strain) are required to fully drive the phase transformation, yielding a target force–displacement ratio of 16.0−16.7 N mm^{-1}. We further clarify that the experimentally achieved force–displacement ratio of the actuator is in good agreement with this target value, confirming that the actuator provides sufficient mechanical output to effectively drive the refrigerant film.

Changes made:

- Add paragraphs in *Supplementary Note 1* to define the target force–displacement ratio based on the mechanical response of the refrigerant film, and added clarification on the agreement between the achieved and target values:

"The target force–displacement ratio in this work was determined based on the mechanical loading requirements of the refrigerant film. Specifically, a transformation force of 5–6 N and a corresponding linear displacement of 300–375 µm (equivalent to 4–5% strain) are required to fully drive the phase transformation. This results in a target force–displacement ratio of 16.0−16.7 N mm^{-1}."

- Added the target force–displacement ratio in the *Discussion* (Page 5 Line 201−202) to facilitate direct comparison between the target and achieved values:

"The force–displacement ratio of the thermal actuation unit is 14.5 N mm^{-1}, which is comparable to the target range (16.0−16.7 N mm^{-1}) and substantially higher than that of a commercially available electromechanical actuator (1.1 N mm^{-1})."

Comment 8: *Supplementary Note 2 conflates efficiency and COP, even though efficiency cannot exceed 100% while COP can, and the authors should revise this section to avoid conceptual confusion.*

Response: We thank the Reviewer for this important comment. We agree that the distinction of theoretical bounds between coefficient of performance (COP) and exergetic efficiency (η_{ex}) should be more clearly defined.

In the revised Supplementary Note 2, we explicitly distinguish these two metrics. The COP is defined as the ratio of cooling output to input energy and is not bounded by unity, whereas η_{ex} is normalized with respect to the corresponding Carnot limit and is therefore bounded by 100%.

Changes made:

- Revised *Supplementary Note 2* to explicitly distinguish the respective theoretical bounds of COP and exergetic efficiency:

"The COP is defined as the ratio of cooling output to input energy and is not bounded by unity, whereas η_{ex} is normalized with respect to the corresponding Carnot limit and is therefore bounded by 100%."

Comment 9: *The notation for temperature differences should be used consistently throughout the manuscript - either T0 - Tc or Tc - T0.*

Response: We thank the Reviewer for this comment regarding notation consistency. We have revised the manuscript to consistently use $T_c - T_0$ to denote the temperature drop. Accordingly, all previously reported values have been updated to reflect this convention.

Changes made:

- Revised *Supplementary Fig. 7a*, *Supplementary Table 3*, and the main text to consistently use $T_c - T_0$ as the notation for temperature drop, with corresponding updates to the sign of reported values:

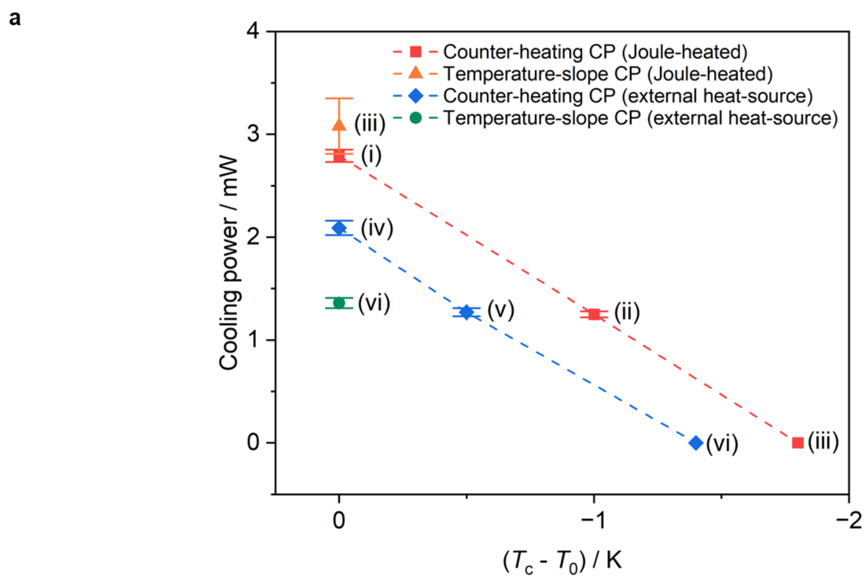

Supplementary Fig. 7. Cooling power under different actuation modes and determination methods. …

Supplementary Table 3. Cooling power of Joule-heated and externally heat-driven elastocaloric systems determined by temperature-slope calculation and direct counter-heating measurement.

Actuation mode	$T_c - T_0$ (K)	Cooling power (temperature-slope) (mW)	Cooling power (counter-heating) (mW)
Joule-heated actuation	0	3.08	2.79
	−1	–	1.25
	−1.8	–	0
External heat-source actuation	0	1.36	2.09
	−0.5	–	1.27
	−1.4	–	0

Cooling power determined using the temperature-slope method is derived from the initial temperature decay rate of the heat source under zero temperature lift conditions. Accordingly, values from the temperature-slope method are only provided for $T_c - T_0 = 0$ K. Cooling power determined using the counter-heating method is obtained as described in the Methods section. "–" indicates not applicable.

Comment 10: *The COPs and exergetic efficiencies in Supplementary Table 4 should be reported with consistent significant digits.*

Response: We thank the Reviewer for this comment regarding formatting consistency. We have revised all COP and exergetic efficiency values in *Supplementary Table 4* and throughout the manuscript to use a consistent format with three significant digits. For values below 0.1, scientific notation is adopted to improve readability.

Changes made:

- Revised COP and exergetic efficiency values in *Supplementary Table 4* and throughout the manuscript to ensure consistent use of significant digits:

Supplementary Table 4. Coefficient of performance (COP) and exergetic efficiency of Joule-heated and externally heat-driven elastocaloric systems under different evaluation criteria. Definitions of COP and exergetic efficiency, including the corresponding input-power bases, are provided in Supplementary Note 2. T_0 denotes the ambient temperature, T_c the heat-source temperature in the cooling unit, and T_h the actuator temperature (Joule-heated case) or the external heat-source temperature.

Evaluation conditions	COP	Exergetic efficiency
Joule heating actuation	evaluated at $T_c - T_0 = 0$ K	evaluated at $T_c - T_0 = -1$ K ($T_c = 294.3$ K)

			(T_0 = 295.3 K) (T_h = 359.7 K)
Temperature-slope method	Cooler (with work recovery)	5.46	–
	Cooler (without work recovery)	2.88	–
	Thermal actuator efficiency (thermal input basis)	~~0.03~~ 3.27×10^{-2}	–
	Thermal actuator efficiency (electrical input basis)	~~0.01~~ 8.37×10^{-3}	–
	Full system (thermal input basis)	~~0.09~~ 9.43×10^{-2}	–
	Full system (electrical input basis)	~~0.02~~ 2.41×10^{-2}	–
	Full system (thermal input basis + auxiliary actuators)	~~0.0008~~ 7.56×10^{-4}	–
	Full system (electrical input basis + auxiliary actuators)	~~0.0007~~ 7.39×10^{-4}	–
Counter-heating method	Cooler (with work recovery)	4.94	4.21 %
	Cooler (without work recovery)	2.61	2.22 %
	Thermal actuator efficiency (thermal input basis)	~~0.03~~ 3.27×10^{-2}	3.27 %
	Thermal actuator efficiency (electrical input basis)	~~0.01~~ 8.37×10^{-3}	~~0.84 %~~ 0.837 %
	Full system (thermal input basis)	~~0.09~~ 8.53×10^{-2}	~~0.07 %~~ 7.27×10^{-2} %
	Full system (electrical input basis)	~~0.02~~ 2.18×10^{-2}	~~0.02 %~~ 1.86×10^{-2} %
	Full system (thermal input basis + auxiliary actuators)	~~0.0007~~ 6.85×10^{-4}	~~0.001 %~~ 5.84×10^{-4} %
	Full system (electrical input basis+ auxiliary actuators)	~~0.0007~~ 6.69×10^{-4}	~~0.001 %~~ 5.71×10^{-4} %
External heat-source actuation		evaluated at $T_c - T_0$ = 0 K	evaluated at $T_c - T_0$ = −0.5 K (T_c = 295.1 K) (T_0 = 295.6 K)

			(T_h = 403.2 K)
Temperature-slope method	Cooler (with work recovery)	2.31	–
	Cooler (without work recovery)	1.50	–
	Thermal actuator efficiency (electrical input basis)	~~0.0024~~ 2.43×10^{-3}	–
	Full system (electrical input basis)	~~0.0036~~ 3.63×10^{-3}	–
	Full system (electrical input basis+ auxiliary actuators)	~~0.0002~~ 2.05×10^{-4}	–
Counter-heating method	Cooler (with work recovery)	3.55	1.37 %
	Cooler without work recovery	2.31	~~0.89 %~~ 0.892 %
	Thermal actuator efficiency (electrical input basis)	~~0.0024~~ 2.43×10^{-3}	~~0.24 %~~ 0.243 %
	Full system (electrical input basis)	~~0.0056~~ 5.60×10^{-3}	~~0.002 %~~ 2.16×10^{-3} %
	Full system (electrical input basis+ auxiliary actuators)	~~0.0003~~ 3.17×10^{-4}	~~< 0.001 %~~ 1.22×10^{-4} %

Reviewer 3's and 4's comments

The authors have adequately addressed the concerns raised during the previous review process. They have incorporated a direct heat source to activate the actuator, clarified the significant discrepancy between device-level and material-level temperature variations, analyzed the heat transfer rates among different components, and demonstrated the mechanical operation and stability of the device. Additionally, they have supplied supplementary details regarding precise device dimensions, comprehensive calculations of cooling power, measurements of cooling temperature on the cold side, and temperature lift assessments. Accordingly, this paper is now suitable for publication in Nature Energy.

Response: We sincerely thank the Reviewer for the positive evaluation of our work and for recognizing the improvements made in the revised manuscript. We greatly appreciate the constructive feedback provided during the review process, which has helped us strengthen the clarity and quality of the manuscript.

Response Letter

We sincerely thank the Editor and the Reviewers for their careful evaluation of our manuscript entitled: “*Heat-driven Elastocaloric Cooling using Shape Memory Films*”. We greatly appreciate the constructive comments, which have helped us improve the clarity, rigor, and positioning of the manuscript.

We have carefully addressed all points raised by the reviewers. Reviewer comments are reproduced in **blue**. Our responses are provided in **black**. Revisions made in the manuscript are shown in **red**.

Below we respond to each comment in detail.

Reviewer 2's comments

The authors have addressed my comments but two revisions are not satisfactory.

Response: We sincerely thank the Reviewer for the careful evaluation of our manuscript and for the constructive and detailed feedback. We appreciate the recognition of the improvements made in the revised version. We have carefully addressed all points raised and revised the manuscript accordingly. Detailed responses to each comment are provided below.

Comment 1: *The new video 4 is helpful, but for consistency, please also add the video of the refrigerant film in the case of external heat source.*

Response: We thank the Reviewer for this suggestion regarding consistency. Following this recommendation, we have added *Supplementary Video 5* showing the operation of the cooling unit in external heat-source-driven configuration.

Changes made:

- Added *Supplementary Video 5* showing the operation of the cooling unit in external heat-source-driven configuration.
- Updated the Discussion section (Page 6, Line 250-252) to reference the new video:

"The operations of the external heat-source-driven actuation unit and the cooling unit in such configuration are shown in Supplementary Video 4 and 5.".

Comment 2: *The added transient data in supplementary fig. 7b is useful. Based on those trends, the temperature span is still developing and full cyclic equilibrium is not reached yet. Why would the authors stop testing prematurely? Please provide relevant information and it will be beneficial to the field.*

Response: We thank the Reviewer for the careful observation and this valuable comment. We agree that in Supplementary Figure 7b, a slight trend is still visible at the end of the measurement. However, given that the final temperature change rate is negligibly small compared to the overall temperature development, the system has already reached a practical steady state for the purpose of this measurement. For clarification, we have provided detailed explanations below and revised the Methods section accordingly to avoid possible misunderstandings.

- By analyzing the temperature evolution profile of the heat source, we calculated that the rate of temperature changing rate at the end of the test is only 0.01 K/s, which is negligible and does not further contribute to a measurable temperature span.
- From the long-term stability test shown in Supplementary Figure 14a, the temperature span already saturates within the initial 22 s, and no noticeable temperature change is observed thereafter. Therefore, the 24 s runtime was selected as the general testing criterion.
- To have consistency throughout this work, all experiments on the coupled device were conducted with a 24 s runtime (except for the long-term stability test, where an extended measurement time was introduced on purpose). Thus, utilizing this identical runtime ensures our cooling power measurements remain comparable and representative while avoiding additional errors and side effects.

Changes made:

- Revised the *Methods* section (Page 12 Line 507–510) to explicitly explain the selection of 24 s runtime in the counter-heating cooling power measurement.

"All measurements are conducted under 24 s runtime to ensure consistency with other tests throughout this work. The remaining temperature changing rate at the end of the measurement is negligibly small and the temperature span development has reached a steady state within the timeframe."